Multiple High-Order Cumulants-Based Spectrum Sensing in Full-Duplex-Enabled Cognitive IoT Networks

Danyang Wang, *Member, IEEE*, Peihan Qi, *Member, IEEE*, Qifan Fu, Ning Zhang, *Senior Member, IEEE*, and Zan Li, *Senior Member, IEEE*

***Abstract*—With unprecedented progress on Internet of Things (IoT), spectrum scarcity becomes even severe with the explosive growth of wireless smart devices. To deal with spectrum scarcity issues, cognitive radio (CR)-enabled IoT has been emerged as a promising solution, which allows IoT devices reusing the underutilized spectrum bands. In this article, we investigate spectrum sensing in CR-IoT, in which full-duplex CR-IoT node can perform spectrum sensing and data transmission concurrently for reducing sensing delay. Two sensing methods are proposed based on multiple high-order cumulants for excavating rich information of the non-Gaussian transmitted signals. Specifically, for the scenarios with a single sensing antenna, we first propose a multiple high-order cumulants-based sensing method (MCS) derived from the likelihood ratio test, which is assumed to be near optimum. The test statistics are derived, respectively, in two cases, i.e., the case only performing sensing and the case performing sensing and transmission simultaneously. Interestingly, the derived two test statistics have same expression, while the corresponding sensing thresholds are different from each other. For the scenarios with multiple sensing antennas, we propose a multiantenna-assisted multiple high-order cumulants-based sensing method (MMCS), which can provide a tradeoff between the computational complexity and sensing performance. We conduct the hypothesis test with Hotelling's T^2-statistic and derive the corresponding sensing threshold. Theoretical performance evaluated by detection probability and computational complexity of the proposed methods are analyzed. Additionally, extensive simulations are provided, which show both the proposed methods can counter the adverse effects of noise uncertainty, and MCS has superiority over MMCS in terms of sensing accuracy.**

***Index Terms*—Cognitive radio (CR), full duplex (FD), high-order cumulants, Internet-of-Things (IoT) networks, multiple sensing antenna, non-Gaussian signal.**

I. Introduction

UNDER the background of large-scale commercial applications of 5G/B5G, the Internet of Things (IoT) that provides a promising platform for various wireless devices and intelligent services has been deemed as an epochal changer for the foreseeable future. Nowadays, there are millions of IoT devices and the total number is forecasted to achieve 80 billion until 2030, with an annual growing rate of about 25%, approximately [1]. On one hand, with sharp increase in diversity of wireless IoT devices from portable facilities to ponderous equipment, the requirement of spectrum resources is also proliferating [2]. On the other hand, as a natural and nonrenewable resources, spectrum resources are considered to be limited. Thus, a conflict exists between the proliferating requirement of spectrum resources and the limitation of spectrum resources, which yields to a spectrum scarcity issue [3]. To deal with this issue, cognitive radio (CR) has been introduced into industrial IoT aiming at improving spectrum efficiency [4], [5]. The CR technology allows secondary IoT systems opportunistically to exploit the available underutilized spectrum by adjusting their transmission modes while guaranteeing a certain level interference to primary IoT systems [6]–[8].

Spectrum sensing has been featured as a key component of CR, which aims to find the spectrum hole timely and accurately [9]–[11]. In traditional cognitive IoT networks, two drawbacks exist when adopting periodic spectrum sensing strategy at the secondary sensing node with half-duplex (HD) mode. First, when the secondary IoT user performing spectrum sensing with HD mode, it fails to protect primary IoT system properly from being harmfully interfered. Since the secondary IoT system cannot perform spectrum sensing during data transmission period such that reaccessing primary IoT users cannot be realized timely, especially when the primary IoT users exploit nontime-slotted (NTS) transmission strategy, which is very common in practice [12]. Second, the optimal sensing duration in the HD mode is usually difficult to determine. A long-sensing duration provides an accurate sensing performance, while resulting in a lower throughput of the secondary IoT system. Inversely, a short sensing duration means

Manuscript received October 30, 2020; revised January 10, 2021; accepted January 27, 2021. Date of publication February 1, 2021; date of current version May 21, 2021. This work was supported in part by the National Natural Science Foundations of China under Grant 61901328; in part by the China Postdoctoral Science Foundation under Grant 2019M653558 and Grant 2018M631122; in part by the National Natural Science Foundation for Distinguished Young Scholar under Grant 61825104; in part by the Key Project of National Natural Science Foundation of China under Grant 61631015; and in part by the University Innovation Platform Project under Grant 2019921815KYPT009JC011. This article was presented in part at IEEE International Conference on Communications Workshops, Dublin, Ireland, 2020. *(Corresponding author: Peihan Qi.)*

Danyang Wang, Peihan Qi, Qifan Fu, and Zan Li are with the State Key Laboratory of Integrated Service Networks, School of Telecommunications Engineering, Xidian University, Xi'an 710071, China (e-mail: dywang@xidian.edu.cn; phqi@xidian.edu.cn; qffu@stu.xidian.edu.cn; zanli@xidian.edu.cn).

Ning Zhang is with the Department of Electrical and Computer Engineering, University of Windsor, Windsor, ON N9B 3P4, Canada (e-mail: ning.zhang@uwindsor.ca).

Digital Object Identifier 10.1109/JIOT.2021.3055782

more time can allocate to data transmission, while the sensing accuracy may degrade and the interference to primary IoT users will increase inevitably [13]. The above-mentioned two drawbacks can be eliminated by combining full-duplex (FD) technology into cognitive IoT networks. With FD technology, secondary IoT system can enable spectrum sensing continuously and transmit message simultaneously, which greatly reduces the interference to primary IoT users and improves the spectrum utilization [14]. The residual self-interference makes combining CR with FD technique intricately. With the help of mature self-interference suppression (SIS) techniques, such as antenna suppression [15], [16], analog suppression [17], and digital suppression [18], residual self-interference can reach an acceptable range [19]–[21].

Besides the adverse effects of residual self-interference come along with the application of FD technology, spectrum sensing is still facing great challenges from the non-Gaussian property of transmitted signals and uncertainty of received noise. In practice, most of the existing systems adopt non-Gaussian signals, such as pulse signals [22], phase-shift keying (PSK) signals [23], *M*-quadrature amplitude modulation (M-QAM)-modulated signals [24], etc. These non-Gaussian transmitted signals degrades the sensing performance of traditional energy-based detector dramatically. The noise uncertainty caused by the non-ideality at receiver device may result in an "SNR" wall, which means below a certain signal-to-noise ratio (SNR) threshold, at least one of the error probabilities, i.e., false-alarm probability and miss detection probability can become worse than 1/2 [25]. Moreover, the residual self-interference in FD-enabled cognitive IoT system enlarges the uncertainty of received noise, which further deteriorates the sensing performance of traditional detectors.

To address the above-mentioned challenges, in this article, we exploit high-order statistics of received signals to carry out spectrum sensing efficiently in the FD-enabled cognitive IoT network. Two spectrum sensing methods, namely, multiple high-order cumulants-based spectrum sensing (MCS) method and multiantenna assisted multiple high-order cumulants-based spectrum sensing (MMCS) method, are proposed. Furthermore, two cases are considered according to whether the cognitive IoT user is transmitting or not when performing sensing. Specifically, when the FD cognitive node equipped with a single sensing antenna, the MCS method is designed with the likelihood ratio test (LRT), which is considered effective in the absence of prior information [26]. Based on the Neyman–Pearson (NP) criterion, the closed-form expression of the decision threshold is obtained. As the MCS method is designed under the scenario with only one sensing antenna, it has the characteristics of simple configuration and low hardware overhead. When the FD cognitive node is equipped with multiple sensing antennas, the MMCS method is proposed, whose test statics is given by Hotelling's T^2-statistic. The corresponding decision threshold is derived numerically, and the detection probability are calculated approximately. In particular, the MMCS method offers a tradeoff between the computational complexity and sensing performance for cognitive IoT systems. Because the statistical process is leveraged to estimate the covariance matrix of high-order cumulants, the computational complexity of the MMCS method is greatly reduced at the expense of the hardware overhead of multi-antennas and lower sensing accuracy. Furthermore, both the proposed methods is robust to noise uncertainty. The major contributions of this work are summarized as follows.

1) We propose two spectrum sensing methods, i.e., MCS method and MMCS method, with the non-Gaussian transmitted signals in the FD-enabled cognitive IoT network, for the cases with one and multiple sensing antenna, respectively. Considering that the cumulants higher than the second order for a Gaussian random process is 0, by leveraging multiple high-order cumulants, both methods can excavate the rich statistical characteristics of the non-Gaussian transmission signals from the Gaussian noise whether colored or not, which improves sensing accuracy and robustness.
2) The applicable scenarios of the proposed two methods differ in the number of sensing antennas and the test characteristics of the two methods are also different. The MCS method achieves a greater sensing accuracy and better tolerance to noise uncertainty, with higher computational complexity than the MMCS method. The MMCS method requires low hardware overhead and sacrifices some spectrum sensing precision in exchange for a significant reduction in computational complexity.
3) Simulation results show that the proposed two methods can better mitigate harmful effects brought by noise uncertainty. Moreover, the sensing performance of both proposed methods with the non-Gaussian signals is better than that of the traditional energy domain-based detector (EDD), which widely used in FD cognitive scenario.

The remainder of this article is organized as follows. The system model of FD-enabled cognitive IoT networks is presented in Section II. In Section III, we propose the MCS method and analyze the computational complexity of this method. Then, the MMCS method with low computational cost are proposed in Section IV. Simulation results are provided in Section V. Finally, Section VI concludes this work.

Notation: The boldface lowercase and uppercase letters denote vectors and matrices, respectively. Detailed key parameters and notations are summarized as in Table I.

TABLE I
KEY PARAMETERS AND NOTATIONS

Symbol	Description
η	Self-interference suppression factor
P_p	Transmission power of primary IoT users
P_s	Transmission power of secondary IoT users
ρ	Noise uncertainty factor in dB
M	Number of delay vectors
K	Number of sensing antennas
h_p	Channels from the primary IoT user to secondary IoT user
h_s	Self-interference channel of secondary IoT user
$\mathrm{Pr}_{\mathrm{fa}}$	False alarm probability
Pr_{d}	Detection probability
N	Sample size per sensing antenna
$F_{a,b}^{(c)}$	$\mathcal{F}$ value for central F distribution with a,b degrees of freedom when the probability is equal to c

II. Related Works

FD-enabled and CR-enabled IoT systems are with high-profile in improving spectral efficiency, in which the spectrum sensing acts as a key component [27]–[29]. Recently, there are several researches on EDD, the frequency-domain-based detector (FDD), and spatial-domain-based cooperative detector (SCD), dedicated to realizing FD-enabled and CR-enabled IoT systems. The sensing methods used most often in FD-enabled and CR-enabled IoT systems are EDD, which is credited for low implementation complexity without any prior information of primary IoT user signal. In addition, when the signal to be detected is a Gaussian signal, the EDD is optimal. However, most of the transmitted signals in real applications are non-Gaussian process, and the performance of EDD suffers baneful influence from noise uncertainty as well as other interferences uncertainty [30], [31].

EDD: Deng *et al.* [32] proposed an adaptive weighted sensing strategy. This method assigned larger weights to the newer sample data, so that the test statistics can better reflect the actual state of the primary IoT user. However, this strategy was aimed at the Gaussian transmitted signals without noise uncertainty, which makes it inefficient for non-Gaussian signals. Sharma *et al.* [33] illustrated a novel two phase concurrent sensing and transmission framework aimed at improving the throughput of the secondary system. In one stage, secondary user transmitted with a restricted power while sensing concurrently, and in another stage, the secondary user transmitted with full power budget. Recently, Shehata and Khattab [34] analyzed the performance of FD energy detection, and derived novel expressions of detection probability and false-alarm probability taking into account the experimentally proven Rician statistical nature of the residual self-interference signal [35] instead of the conventional Gaussian statistical nature. Additionally, the authors illustrated that the previously adopted the conventional Gaussian statistical model achieves the lower bound of sensing performance. Moreover, considering that the conventional energy detector cannot distinguish between residual self-interference, primary user signal, and noise, Afifi and Krunz [36] studied a waveform-based sensing scheme in an FD cognitive network. Specifically, the test statistics were constructed by multiplying the received samples by the conjugate of the prior information of the primary user signal known in advance to distinguish different signal types. However, this scheme requires the pattern of the primary signals, which can not be satisfied in realistic sensing scenarios.

FDD: In [37], by leveraging the discrete Fourier transform (DFT) and expectation maximization (EM) algorithm, the authors proposed a frequency-domain cooperative wideband spectrum sensing scheme. In this scheme, based on a binary hypothesis test, the average power of the primary signal was estimated over a wideband frequency spectrum during the sensing interval. Furthermore, the channel occupation was determined without relying on the channel state. However, the estimation of the transmitted power of the primary signals required prior knowledge of channel state information (CSI) and the noise variances at all the cooperative secondary users.

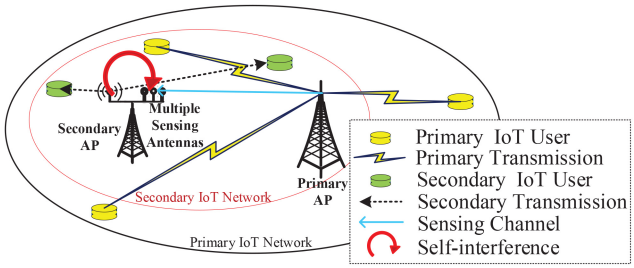

Fig. 1. FD-enabled cognitive IoT networks.

SCD: SCD mainly includes two categories: 1) multiantenna assist detection and 2) multiuser cooperative detection. In [38], a multiantenna-based spectrum sensing method was proposed without prior CSI. By constructing the covariance matrix of multiantenna samples and extracting the eigenvalues of the covariance matrix, the existence of the primary signal was determined based on the generalized likelihood ratio test (GLRT) paradigm. Liu *et al.* [39] proposed a weighted eigenvalue-based LRT for multiantenna CR networks. By using all the eigenvalues of the sample covariance matrix, an optimal detection method based on the likelihood ratio detection was proposed, which requires the priori channel information. Then, considering the practicability, a suboptimal detection scheme was proposed by using the maximum likelihood estimation (MLE) to estimate the noise variance, which can achieve a completely blind sensing. However, the above methods mainly focus on the assumption that the transmitted signals from primary user are Gaussian process. There are rare researches considering the most practical scenarios that the transmitted signals are non-Gaussian process in CR-IoT systems with various heterogeneous resources. Hence, we investigate spectrum sensing scheme in FD-enabled CR-IoT systems with the non-Gaussian transmitted signals.

III. System Model

As shown in Fig. 1, we consider an FD-enabled CR-IoT network, which consists of a primary IoT network and a secondary IoT network. In primary IoT network, there exists a primary access point (AP) serving multiple primary IoT users over the licensed spectrum band. We assume the transmission of primary IoT user is nontime slotted and the spectrum occupation is modeled as an alternating ON/OFF process. The secondary IoT network shares the licensed spectrum band with the primary IoT network by opportunistically accessing the underutilized spectrum when the primary IoT user is inactive. We assume the secondary IoT users are operating with FD mode, such that they can perform spectrum sensing and data transmission simultaneously.

Specifically, the primary IoT users are equipped with single antenna, while each secondary IoT user is equipped with multiple antennas, in which a single antenna is allocated for communication and others are used to perform spectrum sensing. Only when the sensing result shows that the primary licensed spectrum is idle, then the secondary IoT user transmits message to the corresponding secondary AP over the spectrum band. But regardless of whether the secondary IoT

users are in the communication state, their noncommunication functions, such as data collection and data processing are performed normally as they have certain data storage capabilities. Whether or not FD sensing technology is available, secondary IoT users need to identify the spectrum occupancy via spectrum sensing before data transmission. However, compared with traditional HD sensing technology, FD sensing technology ensures that secondary IoT users can carry out spectrum sensing while performing transmission and timely detect the reaccessing of primary IoT users at any time.

According to the operating status of primary IoT users and secondary IoT users, the received signals at the secondary sensing node can be categorized into four different cases. Consequently, four possible hypothetical states, denoted as $\mathcal{H}_0$, $\mathcal{H}_1$, $\mathcal{H}_2$, and $\mathcal{H}_3$ are obtained. To be specific, in hypothesis $\mathcal{H}_0$, the only component of the received signals is background noise, which means neither the primary IoT user nor the secondary IoT user is transmitting; in hypothesis $\mathcal{H}_1$, the received signals consist of primary IoT signals and noise, which indicates that primary IoT user transmits data over the licensed spectrum while the secondary IoT user remains silent; in hypothesis $\mathcal{H}_2$, the components of the received signals include residual self-interference from the secondary IoT user and background noise. That is to say, the primary IoT user does not transmit over the licensed band, and the secondary IoT user utilizes the spectrum for communication while performing spectrum sensing simultaneously for finding the reaccess of the primary IoT user; in hypothesis $\mathcal{H}_3$, the received signals are composed of primary IoT user's signals, residual self-interference of secondary IoT user and background noise. This is because, just as the secondary IoT user is communicating and sensing at the same time, the primary IoT user happens to connect back to the spectrum, such that the secondary IoT system should stop its transmission and release the spectrum to primary IoT system. Noting that the latter two hypotheses are unique to FD cognitive IoT networks compared to HD. Above all, the received signals at the considered hypothesis test model can be expressed as

$$\begin{aligned}
&\mathcal{H}_0 : y(n) = w(n)\\
&\mathcal{H}_1 : y(n) = \sqrt{P_p} h_p(n) x(n) + w(n)\\
&\mathcal{H}_2 : y(n) = \sqrt{\eta P_s} h_s(n) s(n) + w(n)\\
&\mathcal{H}_3 : y(n) = \sqrt{P_p} h_p(n) x(n) + \sqrt{\eta P_s} h_s(n) s(n) + w(n)
\end{aligned} \quad (1)$$

where $w(n)$ represents the additive zero-mean complex-colored Gaussian noise at each sensing antenna of the secondary IoT user, P_p and P_s are the transmit power of the primary IoT user and secondary IoT user, respectively, $x(n)$ and $s(n)$ are the signals transmitted from primary IoT user and secondary IoT user, respectively, h_p and h_s represent the flat Rayleigh fading channels from the primary IoT user to the secondary IoT user and the self-interference channel of secondary IoT user, respectively, and η stands for the SIS ability of secondary IoT user. Specifically, $\eta = 0$ indicates that secondary IoT user can completely suppress the self-interference, and $\eta = 1$ reflects that it does not perform SIS. $\sqrt{\eta P_s} h_s(n) s(n)$ represents the residual self-interference reaching each sensing antenna of secondary IoT user. Furthermore, h_i, $i = p, s$ can be expressed as $|h_i| e^{j\phi_i}$, where $|h_i|$ and ϕ_i are the channel gain and phase elements, respectively. With a flat Rayleigh fading channel, it is generally assumed the channel gain and phase are constant in a very short sensing period.

IV. Multiple High-Order Cumulants-Based Spectrum Sensing Method

In this section, we propose a multiple high-order cumulants-based spectrum sensing scheme in FD-enabled CR-IoT networks with single sensing antenna. First, the estimation and statistical law of high-order cumulants with finite-length samples are introduced, and then we derive the sensing scheme for recognizing the working status of primary IoT user. Finally, the computational complexity of MCS scheme is analyzed in the last section.

A. Estimation of Cumulants With Finite-Length Samples

Definition 1: For a random vector $\boldsymbol{x} = [x_1, x_2, \ldots, x_k]$, the cumulants is defined as the coefficients in the Taylor series expansion of the natural logarithm of the its characteristic function as follows:

$$\begin{aligned}
c_k(\boldsymbol{x}) &\triangleq \mathrm{cum}\{x_1, x_2, \ldots, x_k\}\\
&\triangleq (-j)^k \cdot \left. \frac{\partial^k \ln \Phi(\omega_1, \ldots, \omega_k)}{\partial_{\omega_1} \partial_{\omega_2} \cdots \partial_{\omega_k}} \right|_{\omega_1 = \cdots = \omega_k = 0}
\end{aligned} \quad (2)$$

where $\Phi(\omega_1, \ldots, \omega_k) \triangleq E\{e^{j\omega_1 x_1 + \cdots + j\omega_k x_k}\}$ is the characteristic function of vector $\boldsymbol{x}$ [40, Ch. 1].

Based on Definition 1, considering a discrete-time stationary complex-valued process $y(n)$ with $k-1$ lags $\boldsymbol{\tau} = [\tau_1, \ldots, \tau_{k-1}]$, which is denoted by a random vector $\boldsymbol{y} = [y(n), \ldots, y(n+\tau_{l-1}), y(n+\tau_l), \ldots, y(n+\tau_{k-1})]$. Then, the cumulants of $\boldsymbol{y}$ are defined as

$$u_{ky}(\boldsymbol{\tau}) \triangleq \mathrm{cum}\left\{ \begin{array}{l} \underbrace{y(n), \ldots, y(n+\tau_{l-1})}_{l} \\ \times \underbrace{y^*(n+\tau_l), \ldots, y^*(n+\tau_{k-1})}_{k-l} \end{array} \right\} \quad (3)$$

where * represents the conjugation operation and $0 \le l \le k$. Obviously, for a certain order k, the kth-order cumulants of a complex process are influenced by l. Whereas, the following analyses have applicability to each of l's values

However, as a practical matter, only finite samples can be obtained by sensing antenna in the secondary IoT user. Hence, the estimated high-order cumulant of the finite signal samples $y(n)$, $n = 0, \ldots, N-1$ is calculated as [41, Ch. 2]

$$\hat{u}_{ky}(\tau) = \sum_{\boldsymbol{v}} (-1)^{(m-1)} (m-1)! \hat{\zeta}_{v_1 y} \cdots \hat{\zeta}_{v_p y} \quad (4)$$

where $(v_1, \ldots, v_m)$ is a partition of set $\{1, 2, \ldots, k\}$ with the number of elements included in each partition recorded as m and $\hat{\zeta}_{ky}$ is the estimated kth-order sample moment of the finite-length samplings $y(n)$, calculated by

$$\begin{aligned}
\hat{\zeta}_{ky}(\tau) = \frac{1}{N} \sum_{n=0}^{N-1} &\underbrace{y(n), \ldots, y(n+\tau_{l-1})}_{l}\\
&\times \underbrace{y^*(n+\tau_l), \ldots, y^*(n+\tau_{k-1})}_{k-l}.
\end{aligned} \quad (5)$$

Moreover, according to [42], if $y(n)$ satisfies the assumption $\sum_{\tau_1,\ldots,\tau_{k-1}=-\infty}^{\infty}|\tau_i u_{ky}(\tau)| < +\infty, i \in \{1,\ldots,k-1\}$, then the estimated sample cumulant $\hat{u}_{ky}(\tau)$ is asymptotically unbiased, mean-square sense consistent, and $\sqrt{N}[\hat{u}_{ky}(\tau) - u_{ky}(\tau)]$ obeys an asymptotically complex normal distribution. Furthermore, the estimated covariance between $\sqrt{N}\hat{u}_{k_1y}(\tau)$ and $\sqrt{N}\hat{u}_{k_2y}(\rho)$ is

$$\hat{\mathcal{Q}}_{k_1,k_2}(\tau,\rho) = \sum_{\upsilon_1}\sum_{\upsilon_2}(-1)^{m_1+m_2-2}(m_1-1)!\times(m_2-1)! \times \sum_{l_1=1}^{m_1}\sum_{l_2=1}^{m_2}\prod_{\substack{n_1=1\\ n_1\neq l_1}}^{m_1}\hat{\zeta}_{\omega_{n_1y}}\prod_{\substack{n_2=1\\ n_2\neq l_2}}^{m_2}\hat{\zeta}_{\upsilon_{n_2y}}\hat{\mathcal{D}}_{l_1,l_2}(\tau_{l_1},\tau_{l_2}) \tag{6}$$

where $\hat{\mathcal{D}}_{l_1,l_2}(\tau_{l_1},\tau_{l_2})$ is the estimated asymptotic covariance of $\sqrt{N}\hat{\zeta}_{l_1y}(\tau_{l_1})$ and $\sqrt{N}\hat{\zeta}_{l_2y}(\tau_{l_1})$. Also according to [42], when $y(n)$ satisfies the aforementioned assumption, the sample moment $\hat{\zeta}_{ky}(\tau)$ is also asymptotically unbiased, mean-square sense consistent, i.e.,$\lim_{N\to\infty}\hat{\zeta}_{ky}(\tau) = \zeta_{ky}(\tau)$. Moreover, $\sqrt{N}[\hat{\zeta}_{ky}(\tau) - \zeta_{ky}(\tau)]$ is asymptotically complex normal. In practice, the estimated asymptotic covariance of $\sqrt{N}\hat{\zeta}_{k_1y}(\tau)$ and $\sqrt{N}\hat{\zeta}_{k_2y}(\rho)$ is used and can be expressed as [43]

$$\begin{aligned}&\hat{\mathcal{D}}_{l_1,l_2}(\tau_{l_1},\tau_{l_2})\\ &\triangleq \sum_{\xi} d_s(\xi)\frac{1}{\sum_n d_\pi\left(\frac{n}{N}\right)}\sum_n d_\pi\left(\frac{n+\xi}{N}\right)d_\pi\left(\frac{n}{N}\right)\\ &\quad\times\left[f_{\tau_{l_1}}(n+\xi)-\hat{\zeta}_{f_{\tau_{l_1}}}\right]\left[f^*_{\tau_{l_2}}(n)-\hat{\zeta}^*_{f_{\tau_{l_2}}}\right]\end{aligned} \tag{7}$$

where $d_s(\xi)$ is a symmetric real-valued spectral window with $d_s(0) = 1$, whose length is S, $d_\pi(n)$ is a tapering window of bounder variations that vanishes for $|n| > 1$, and $f_\tau(n)$ and $\hat{\zeta}_{f_\tau}$ are defined as

$$\begin{aligned}f_\tau(n) &\triangleq y(n)y(n+\tau_1)\cdots y(n+\tau_{k-1})\\ \hat{\zeta}_{f_\tau} &\triangleq \frac{\sum_n d_\pi\left(\frac{n}{N}\right)f_\tau(n)}{\sum_n d_\pi\left(\frac{n}{N}\right)}.\end{aligned} \tag{8}$$

B. Statistical Law of High-Order Cumulant

To achieve fine spectrum sensing performance, we use multiple high-order cumulants to exploit the rich statistical features of the received signal. The statistical characteristics of multiple high-order cumulants, which are vital for detection algorithms are also derived. Given M orders vector $\{k_1,\ldots,k_M\}$ and corresponding M lag vectors $\{\boldsymbol{\tau}_1,\ldots,\boldsymbol{\tau}_M\}$ with $\boldsymbol{\tau}_i = [\tau_1,\ldots,\tau_{k_i-1}]$, an $1\times M$-dimension vector of the estimated multiple kth-order cumulants for a finite-length sample data recorded as $\boldsymbol{u}_{ky}(\boldsymbol{\tau}) \triangleq [u_{k_1y}(\boldsymbol{\tau}_1),\ldots,u_{k_My}(\boldsymbol{\tau}_M)]$ is defined, whose corresponding estimated $\hat{\boldsymbol{u}}_{ky}(\boldsymbol{\tau})$ can be expressed as

$$\hat{\boldsymbol{u}}_{ky}(\boldsymbol{\tau}) \triangleq \left[\hat{u}_{k_1y}(\boldsymbol{\tau}_1),\ldots,\hat{u}_{k_My}(\boldsymbol{\tau}_M)\right]. \tag{9}$$

Given multiple different orders and different lags, we can calculate the estimated multiple kth-order cumulants for the received finite-length N sample data. If so, the hypothesis test model expressed in (1) yields as

$$\begin{aligned}\mathcal{H}_0 &: \hat{\boldsymbol{u}}_{ky}(\boldsymbol{\tau}) = \boldsymbol{u}_{kw}(\boldsymbol{\tau}) + \boldsymbol{\varepsilon}^{(N)}_{ky}(\boldsymbol{\tau})\\ \mathcal{H}_1 &: \hat{\boldsymbol{u}}_{ky}(\boldsymbol{\tau}) = P_p^{k/2}\boldsymbol{u}_{kp}(\boldsymbol{\tau}) + \boldsymbol{u}_{kw}(\boldsymbol{\tau}) + \boldsymbol{\varepsilon}^{(N)}_{ky}(\boldsymbol{\tau})\\ \mathcal{H}_2 &: \hat{\boldsymbol{u}}_{ky}(\boldsymbol{\tau}) = (\eta P_s)^{k/2}\boldsymbol{u}_{ks}(\boldsymbol{\tau}) + \boldsymbol{u}_{kw}(\boldsymbol{\tau}) + \boldsymbol{\varepsilon}^{(N)}_{ky}(\boldsymbol{\tau})\\ \mathcal{H}_3 &: \hat{\boldsymbol{u}}_{ky}(\boldsymbol{\tau}) = P_p^{k/2}\boldsymbol{u}_{kp}(\boldsymbol{\tau}) + (\eta P_s)^{k/2}\boldsymbol{u}_{ks}(\boldsymbol{\tau})\\ &\qquad + \boldsymbol{u}_{kw}(\boldsymbol{\tau}) + \boldsymbol{\varepsilon}^{(N)}_{ky}(\boldsymbol{\tau})\end{aligned} \tag{10}$$

where $\boldsymbol{u}_{kp}(\boldsymbol{\tau})$, $\boldsymbol{u}_{ks}(\boldsymbol{\tau})$, and $\boldsymbol{\varepsilon}^{(N)}_{ky}(\boldsymbol{\tau})$ are separately defined as

$$\begin{aligned}\boldsymbol{u}_{kp}(\boldsymbol{\tau}) &= \left[u_{k_1p,h_p}(\boldsymbol{\tau}_1),\ldots,u_{k_Mp,h_p}(\boldsymbol{\tau}_M)\right]\\ \boldsymbol{u}_{ks}(\boldsymbol{\tau}) &= \left[u_{k_1s,h_s}(\boldsymbol{\tau}_1),\ldots,u_{k_Ms,h_s}(\boldsymbol{\tau}_M)\right]\\ \boldsymbol{\varepsilon}^{(N)}_{ky}(\boldsymbol{\tau}) &= \left[\varepsilon^{(N)}_{k_1y}(\boldsymbol{\tau}_1),\ldots,\varepsilon^{(N)}_{k_My}(\boldsymbol{\tau}_M)\right].\end{aligned}$$

Additionally, $\boldsymbol{\varepsilon}^{(N)}_{ky}(\boldsymbol{\tau})$ represents the estimation error, which goes to 0 gradually when N tends to infinity, and

$$\begin{aligned}u_{k_ip,h_p}(\boldsymbol{\tau}_i) &= |h_p|^{k_i}e^{j\phi_p(2l_i-k_i)}u_{k_ip}(\boldsymbol{\tau}_i)\\ u_{k_is,h_s}(\boldsymbol{\tau}_i) &= |h_s|^{k_i}e^{j\phi_s(2l_i-k_i)}u_{k_is}(\boldsymbol{\tau}_i).\end{aligned}$$

If $w(n)$ is the Gaussian noise, i.e., a Gaussian random process, its cumulants higher than the second order are all 0, whether it is colored noise or not. Whereas, for a non-Gaussian stochastic process, its cumulants are not 0. When $y(n)$ is zero-mean (if not, one can estimate and subtract the mean), given a certain k order and delay parameter vector $\boldsymbol{\tau} = [\tau_1,\ldots,\tau_M]$, we can assume that $\boldsymbol{u}_{kp}(\boldsymbol{\tau})$ and $\boldsymbol{u}_{ks}(\boldsymbol{\tau})$ exist while $\boldsymbol{u}_{kw}(\boldsymbol{\tau})$ vanish. For simplicity, the delay parameter vector $\boldsymbol{\tau}$ is omitted in the following discussion. Specifically, $\hat{\boldsymbol{u}}_{ky}$, $\boldsymbol{u}_{kp}$, and $\boldsymbol{u}_{ks}$ are used to indicate $\hat{\boldsymbol{u}}_{ky}(\boldsymbol{\tau})$, $\boldsymbol{u}_{kp}(\boldsymbol{\tau})$, and $\boldsymbol{u}_{ks}(\boldsymbol{\tau})$, respectively. Therefore, (10) can be rewritten as

$$\begin{aligned}\mathcal{H}_0 &: \hat{\boldsymbol{u}}_{ky} = \boldsymbol{\varepsilon}^{(N)}_{ky}\\ \mathcal{H}_1 &: \hat{\boldsymbol{u}}_{ky} = P_p^{k/2}\boldsymbol{u}_{kp} + \boldsymbol{\varepsilon}^{(N)}_{ky}\\ \mathcal{H}_2 &: \hat{\boldsymbol{u}}_{ky} = (\eta P_s)^{k/2}\boldsymbol{u}_{ks} + \boldsymbol{\varepsilon}^{(N)}_{ky}\\ \mathcal{H}_3 &: \hat{\boldsymbol{u}}_{ky} = P_p^{k/2}\boldsymbol{u}_{kp} + (\eta P_s)^{k/2}\boldsymbol{u}_{ks} + \boldsymbol{\varepsilon}^{(N)}_{ky}.\end{aligned} \tag{11}$$

Since the secondary IoT user has two working states: 1) "sensing only" and 2) "transmitting and sensing," which can be distinguished by the secondary IoT user itself as whether having ongoing transmission service, the aforementioned four hypotheses in (11) can be divided into two cases based on whether the secondary IoT user transmitting or not. When the secondary IoT user has no transmission service and performs spectrum sensing only, just like the traditional HD sensing technology, working state of the primary IoT user is identified via $\mathcal{H}_0$ and $\mathcal{H}_1$, which is termed case I; when the secondary IoT user simultaneously senses and transmits with the assistance of FD technology, the working state of the primary IoT user is identified via $\mathcal{H}_2$ and $\mathcal{H}_3$, which is termed case II.

In Case I: the secondary IoT user senses only without transmission service, then the hypothesis test model in case I includes

$$\begin{aligned}\mathcal{H}_0 &: \hat{\boldsymbol{u}}_{ky} = \boldsymbol{\varepsilon}^{(N)}_{ky}\\ \mathcal{H}_1 &: \hat{\boldsymbol{u}}_{ky} = P_p^{k/2}\boldsymbol{u}_{kp} + \boldsymbol{\varepsilon}^{(N)}_{ky}.\end{aligned} \tag{12}$$

Notice that $\sqrt{N}[\hat{\boldsymbol{u}}_{ky} - \boldsymbol{u}_{ky}] = \sqrt{N}[\hat{\boldsymbol{u}}_{ky} - P_p^{k/2}\boldsymbol{u}_{kp}]$ is asymptotically normal on the grounds of the asymptotically normal

distribution obeyed by $\sqrt{N}[\hat{u}_{ky}(\boldsymbol{\tau}) - u_{ky}(\boldsymbol{\tau})]$, and the (m, n)th entry of the estimative covariance matrix $\boldsymbol{\Sigma}$ of $\hat{\boldsymbol{u}}_{ky}$ can be calculated by using (6). Furthermore, the probability density function (PDF) of $\hat{\boldsymbol{u}}_{ky}$ in case I can be expressed as

$$p\big(\hat{\boldsymbol{u}}_{ky}|\mathcal{H}_i\big) = \frac{1}{\pi^M|\boldsymbol{\Sigma}|} \times \exp\Big\{-\Xi_p \boldsymbol{\Sigma}^{-1} \Xi_p^H\Big\} \tag{13}$$

where $\Xi_p = \hat{\boldsymbol{u}}_{ky} - iP_p^{k/2}\boldsymbol{u}_{kp}$ and $i = 0, 1$.

In Case II: The secondary IoT user senses and transmits simultaneously based on FD technology, and the hypothesis test model in case II includes

$$\begin{aligned}\mathcal{H}_2{:}\hat{\boldsymbol{u}}_{ky} &= (\eta P_s)^{k/2}\boldsymbol{u}_{ks} + \boldsymbol{\varepsilon}_{ky}^{(N)}\\ \mathcal{H}_3{:}\hat{\boldsymbol{u}}_{ky} &= P_p^{k/2}\boldsymbol{u}_{kp} + (\eta P_s)^{k/2}\boldsymbol{u}_{ks} + \boldsymbol{\varepsilon}_{ky}^{(N)}.\end{aligned} \tag{14}$$

Similar to case I, the PDF of $\hat{\boldsymbol{u}}_{ky}$ in case II can be expressed as

$$p\big(\hat{\boldsymbol{u}}_{ky}|\mathcal{H}_r\big) = \frac{1}{\pi^M|\boldsymbol{\Sigma}|} \times \exp\Big\{-\Xi_s \boldsymbol{\Sigma}^{-1} \Xi_s^H\Big\} \tag{15}$$

where $\Xi_s = \hat{\boldsymbol{u}}_{ky} - (r-2)P_p^{k/2}\boldsymbol{u}_{kp} - (\eta P_s)^{k/2}\boldsymbol{u}_{ks}$ and $r = 2, 3$.

C. Detection of Primary IoT User's Working State

To determine whether the primary IoT user is in a communication state, it is necessary to carry out LRT in the case of unknown prior information, which is often the actual situation in practical situations. Then, the likelihood ratio decision rule between two hypotheses can be written as

$$\psi\big(\hat{\boldsymbol{u}}_{ky}\big) = \frac{P\big(\hat{\boldsymbol{u}}_{ky}|\mathcal{H}_{\text{on}}\big)}{P\big(\hat{\boldsymbol{u}}_{ky}|\mathcal{H}_{\text{off}}\big)} \underset{\mathcal{H}_{\text{off}}}{\overset{\mathcal{H}_{\text{on}}}{\gtrless}} \gamma \tag{16}$$

where γ is the predetermined threshold of LRT.

In case I, substituting (13) into (16) and taking natural logarithm processing to (16), the decision rule in case I can be constructed as

$$P_p^{k/2}\boldsymbol{u}_{kp}^H\boldsymbol{\Sigma}^{-1}\hat{\boldsymbol{u}}_{ky} \underset{\mathcal{H}_0}{\overset{\mathcal{H}_1}{\gtrless}} \frac{1}{2}\Big(\ln\gamma_1 + P_p^k\boldsymbol{u}_{kp}^H\boldsymbol{\Sigma}^{-1}\boldsymbol{u}_{kp}\Big). \tag{17}$$

From (17), the test statistics $L_{\text{caseI}}^{\text{LRT}}$ and detection threshold $\Omega_{\text{caseI}}^{\text{LRT}}$ are set separately as

$$L_{\text{caseI}}^{\text{LRT}} = P_p^{k/2}\boldsymbol{u}_{kp}^H\boldsymbol{\Sigma}^{-1}\hat{\boldsymbol{u}}_{ky} \tag{18}$$

$$\Omega_{\text{caseI}}^{\text{LRT}} = \frac{1}{2}\Big(\ln\gamma_1 + P_p^k\boldsymbol{u}_{kp}^H\boldsymbol{\Sigma}^{-1}\boldsymbol{u}_{kp}\Big). \tag{19}$$

Consider that the test statistic $L_{\text{caseI}}^{\text{LRT}}$ is the weighted sum of a series of Gaussian random variables; therefore, $L_{\text{caseI}}^{\text{LRT}}$ obeys the Gaussian distribution under hypothesis $\mathcal{H}_i$, $i = 0, 1$, i.e.,

$$\mathcal{H}_i{:}\ L_{\text{caseI}}^{\text{LRT}} \sim \mathcal{N}\Big(iP_p^k\boldsymbol{u}_{kp}^H\boldsymbol{\Sigma}^{-1}\boldsymbol{u}_{kp}, P_p^k\boldsymbol{u}_{kp}^H\boldsymbol{\Sigma}^{-1}\boldsymbol{u}_{kp}\Big). \tag{20}$$

Thus, the detection probability and false-alarm probability can be calculated, respectively, as

$$\begin{aligned}\text{Pr}_d(\gamma_1) &= \text{Pr}(\mathcal{H}_{\text{on}}|\mathcal{H}_{\text{on}}) = \text{Pr}\big(L_{\text{caseI}}^{\text{LRT}} > \Omega_{\text{caseI}}^{\text{LRT}}|\mathcal{H}_1\big)\\ &= Q\left(\frac{\Omega_{\text{caseI}}^{\text{LRT}} - P_p^k\boldsymbol{u}_{kp}^H\boldsymbol{\Sigma}^{-1}\boldsymbol{u}_{kp}}{P_p^{k/2}\sqrt{\boldsymbol{u}_{kp}^H\boldsymbol{\Sigma}^{-1}\boldsymbol{u}_{kp}}}\right)\\ &= Q\left(\frac{\ln\gamma_1}{2d} - \frac{d}{2}\right)\end{aligned} \tag{21}$$

$$\begin{aligned}\text{Pr}_{fa}(\gamma_1) &= \text{Pr}(\mathcal{H}_{\text{on}}|\mathcal{H}_{\text{off}}) = \text{Pr}\big(L_{\text{caseI}}^{\text{LRT}} > \Omega_{\text{caseI}}^{\text{LRT}}|\mathcal{H}_0\big)\\ &= Q\left(\frac{\Omega_{\text{caseI}}^{\text{LRT}}}{P_p^{k/2}\sqrt{\boldsymbol{u}_{kp}^H\boldsymbol{\Sigma}^{-1}\boldsymbol{u}_{kp}}}\right) = Q\left(\frac{\ln\gamma_1}{2d} + \frac{d}{2}\right)\end{aligned} \tag{22}$$

where $d = P_p^{k/2}\sqrt{\boldsymbol{u}_{kp}^H\boldsymbol{\Sigma}^{-1}\boldsymbol{u}_{kp}}$. Particularly, d^2 is the sample-squared distance between the means of two hypotheses, which represents the maximum separation in the samples from two hypotheses [44, Ch. 11].

In many practical situations, such as radars and sonars, among other signals detections, we can neither predict prior probability $\text{Pr}(\mathcal{H}_{\text{on}})$ and $\text{Pr}(\mathcal{H}_{\text{off}})$ nor preset cost factors $c_{i,j}$ for various decision results. For this kind of situation, to ensure that information processing system can effectively deal with useful data and avoid too many false data that affect the working efficiency being input into information processing system, while ensuring information processing system access to useful data as much as possible, which requires the decision error probability $\text{Pr}_{fa} = \text{Pr}(\mathcal{H}_{\text{on}}|\mathcal{H}_{\text{off}})$ as small as possible and the correct detection probability $\text{Pr}_d = \text{Pr}(\mathcal{H}_{\text{on}}|\mathcal{H}_{\text{on}})$ as large as possible. In addition, for a certain SNR, the increase in Pr_d will lead to a subsequent increase in Pr_{fa}. Therefore, to control false-alarm probability as small as possible, we adopt the NP criterion to make the maximum Pr_d under the constraint condition of $\text{Pr}_{fa} = \delta$ [26, Ch. 3]. If we set Pr_{fa} to be less than δ_I, then the corresponding detection threshold can be calculated as

$$\gamma_1^{\text{NP}} = \exp\Big(2dQ^{-1}(\delta_{\text{I}}) - d^2\Big). \tag{23}$$

Hence, the detection probability of case I can be derived as

$$\text{Pr}_{\text{d1}} = Q\Big(Q^{-1}(\delta_{\text{I}}) - d\Big). \tag{24}$$

In Case II, combining (15) with (16), meanwhile, treating both sides of (16) with natural logarithm processing, the decision rule in case II can be constructed as

$$\begin{aligned}&P_p^{k/2}\boldsymbol{u}_{kp}^H\boldsymbol{\Sigma}^{-1}\hat{\boldsymbol{u}}_{ky} \underset{\mathcal{H}_2}{\overset{\mathcal{H}_3}{\gtrless}}\\ &\frac{1}{2}\Big(\ln\gamma_2 + P_p^k\boldsymbol{u}_{kp}^H\boldsymbol{\Sigma}^{-1}\boldsymbol{u}_{kp} + 2\big(\eta P_p P_s\big)^{k/2}\boldsymbol{u}_{ks}^H\boldsymbol{\Sigma}^{-1}\boldsymbol{u}_{kp}\Big).\end{aligned} \tag{25}$$

From (25), the test statistics $L_{\text{caseII}}^{\text{LRT}}$ and detection threshold $\Omega_{\text{caseII}}^{\text{LRT}}$ are set separately as

$$L_{\text{caseII}}^{\text{LRT}} = P_p^{k/2}\boldsymbol{u}_{kp}^H\boldsymbol{\Sigma}^{-1}\hat{\boldsymbol{u}}_{ky} \tag{26}$$

$$\Omega_{\text{caseII}}^{\text{LRT}} = \frac{1}{2}\Big(\ln\gamma_2 + P_p^k\boldsymbol{u}_{kp}^H\boldsymbol{\Sigma}^{-1}\boldsymbol{u}_{kp} + 2\big(\eta P_p P_s\big)^{k/2}\boldsymbol{u}_{ks}^H\boldsymbol{\Sigma}^{-1}\boldsymbol{u}_{kp}\Big). \tag{27}$$

Interestingly, the test statistics have the same form in both cases, but they obey different distributions. It is obvious that $L_{\text{caseII}}^{\text{LRT}}$ obeys the Gaussian distribution under hypothesis $\mathcal{H}_r$, $r = 2, 3$, i.e.,

$$\begin{aligned}\mathcal{H}_r{:}\ L_{\text{caseII}}^{\text{LRT}} \sim \mathcal{N}\Big(&P_p^{k/2}\boldsymbol{u}_{kp}^H\boldsymbol{\Sigma}^{-1}\Big((r-2)P_p^{k/2}\boldsymbol{u}_{kp}\\ &+ (\eta P_s)^{k/2}\boldsymbol{u}_{ks}\Big)P_p^k\boldsymbol{u}_{kp}^H\boldsymbol{\Sigma}^{-1}\boldsymbol{u}_{kp}\Big).\end{aligned} \tag{28}$$

Hence, the detection probability and false-alarm probability can be derived, respectively, as

$$\begin{aligned}\mathrm{Pr}_d(\gamma_2) &= \mathrm{Pr}(\mathcal{H}_{\mathrm{on}}|\mathcal{H}_{\mathrm{on}}) = \mathrm{Pr}\big(L_{\mathrm{caseII}}^{\mathrm{LRT}} > \Omega_{\mathrm{caseII}}^{\mathrm{LRT}}|\mathcal{H}_3\big) \\ &= Q\left(\frac{\Omega_{\mathrm{caseII}}^{\mathrm{LRT}} - P_p^k \boldsymbol{u}_{kp}^H \boldsymbol{\Sigma}^{-1}\boldsymbol{u}_{kp} - \big(\eta P_p P_s\big)^{k/2}\boldsymbol{u}_{ks}^H\boldsymbol{\Sigma}^{-1}\boldsymbol{u}_{kp}}{P_p^{k/2}\sqrt{\boldsymbol{u}_{kp}^H\boldsymbol{\Sigma}^{-1}\boldsymbol{u}_{kp}}}\right) \\ &= Q\left(\frac{\ln\gamma_2}{2d} - \frac{d}{2}\right) \end{aligned} \tag{29}$$

$$\begin{aligned}\mathrm{Pr}_{fa}(\gamma_2) &= \mathrm{Pr}(\mathcal{H}_{\mathrm{on}}|\mathcal{H}_{\mathrm{off}}) = \mathrm{Pr}\big(L_{\mathrm{caseII}}^{\mathrm{LRT}} > \Omega_{\mathrm{caseII}}^{\mathrm{LRT}}|\mathcal{H}_2\big) \\ &= Q\left(\frac{\Omega_{\mathrm{caseII}}^{\mathrm{LRT}} - \big(\eta P_p P_s\big)^{k/2}\boldsymbol{u}_{ks}^H\boldsymbol{\Sigma}^{-1}\boldsymbol{u}_{kp}}{P_p^{k/2}\sqrt{\boldsymbol{u}_{kp}^H\boldsymbol{\Sigma}^{-1}\boldsymbol{u}_{kp}}}\right) \\ &= Q\left(\frac{\ln\gamma_2}{2d} + \frac{d}{2}\right) \end{aligned} \tag{30}$$

where $d = P_p^{k/2}\sqrt{\boldsymbol{u}_{kp}^H\boldsymbol{\Sigma}^{-1}\boldsymbol{u}_{kp}}$ as well.

To control the false-alarm probability as small as possible, the NP criterion is used. If we set Pr_{fa} to be less than δ_{II}, and from (30), the corresponding detection threshold in case II can be calculated as

$$\gamma_2^{\mathrm{NP}} = \exp\Big(2dQ^{-1}(\delta_{II}) - d^2\Big). \tag{31}$$

Hence, the detection probability of case II can be simplified as

$$\mathrm{Pr}_{\mathrm{d2}} = Q\Big(Q^{-1}(\delta_{II}) - d\Big). \tag{32}$$

Note that the detection probability derived under the NP criterion here is the same as that in case I in format as long as $\delta_{\mathrm{I}} = \delta_{II}$.

In summary, the proposed MCS detection scheme has four steps as given as follows.

Step 1: Based on N samples of each sensing antenna, given M orders vectors $\{k_1, \ldots, k_M\}$ and corresponding M lag vectors $\{\boldsymbol{\tau}_1, \ldots, \boldsymbol{\tau}_M\}$, the estimated cumulants of received signals from the secondary IoT user can be constructed according to (4) and (9). Based on the working status of the secondary IoT user, confirm whether this test process is in case I or case II.

Step 2: Evaluate the estimation of covariance matrix $\boldsymbol{\Sigma}$ by using (6).

Step 3: Construct test statistics $L_{\mathrm{caseI}}^{\mathrm{LRT}}$ in case I or $L_{\mathrm{caseII}}^{\mathrm{LRT}}$ in case II according to (18) or (26), respectively.

Step 4: Preset false-alarm probability Pr_{fa}. Then, set up the threshold γ_1^{NP} or γ_2^{NP} according to (23) or (31) with Pr_{fa} preset. By comparing test statistics and threshold, we can determine the working state of the primary IoT user. The estimated detection probability can be calculated by (24) or (32).

D. Computational Complexity of MCS Scheme

With regard to the computational complexity of the MCS scheme, first, it is necessary to perform $\sum_{i=1}^{M} v_i(k_i - 1)N$ multiplications and $\sum_{i=1}^{M}\sum_{g=1}^{v_i} m_g(N-1)$ additions to figure out the estimated k-order cumulants $\hat{\boldsymbol{u}}_{ky}(\boldsymbol{\tau})$. Then, $\sum_{r=1}^{M}\sum_{z=1}^{M}\sum_{i=1}^{V_r}\sum_{g=1}^{V_z}\sum_{l_1=1}^{m_i}\sum_{l_2=1}^{m_g}[(\sum_{\substack{q_1=1\\q_1\neq l_1}}^{m_i} v_{q1} + \sum_{\substack{q_2=1\\q_2\neq l_2}}^{m_g} v_{q2}) \times (N-1) + S(v_{l_1} + v_{l_2} + 4)N]$ multiplications and $\sum_{r=1}^{M}\sum_{z=1}^{M}\sum_{i=1}^{V_r}\sum_{g=1}^{V_z}\sum_{l_1=1}^{m_i}\sum_{l_2=1}^{m_g}[(m_i + m_g - 2)(N-1) + S + 4N]$ additions are necessary to calculate the estimate of the covariance matrix $\boldsymbol{\Sigma}$. Hence, the computational complexity of the MCS scheme is very high. Specifically, the computational complexity mainly comes from the estimation of covariance matrix.

V. Multiple Antenna Enabled Multiple High-Order Cumulants-Based Spectrum Sensing Method

Though the MCS scheme is derived by LRT, which is suitable for the practical scenario without prior information, the complexity of this scheme is very high mainly due to calculating the estimated covariance matrix by (6). If multiple sensing antennas are available at the secondary IoT user, we can make hypothesis testing decisions based on the statistical characteristics of the samples in each hypothesis. In the case of multiantenna spectrum sensing, considering that the high-order cumulants calculated by the samples in each case have the statistical characteristics of the same variance and different mean values, to reduce the computational complexity, we adopt Hotelling's T^2-statistic to construct hypothesis tests to determine whether the primary IoT user is working or not. Hence, the MMCS scheme is proposed in FD-enabled CR-IoT networks. We obtain the closed-form solution of the decision threshold and then derive the closed-form expression of the estimated detection probability by a suitable Gaussian approximation. Similarly, the computational complexity of the MMCS scheme is analyzed in the last section, and the computational complexity of the two proposed methods is also compared.

A. Estimated Cumulants of Samples From Multiple Sensing Antennas

Consider that the secondary IoT user is outfitted with single transmitting antenna as well as K sensing antennas. We assume that each sensing antenna allocates N samples in one sensing duration. Thus, the received sample matrix can be presented as $\boldsymbol{\Upsilon} = [\boldsymbol{y}_1, \boldsymbol{y}_2, \ldots, \boldsymbol{y}_K]^T$, where $\boldsymbol{y}_i = [y_i(0), \ldots, y_i(N-1)]$ is the received N samples at the ith sensing antenna.

Then, under K sensing antennas circumstances, (1) yields

$$\begin{aligned}\mathcal{H}_0 &: \boldsymbol{\Upsilon} = \ \mathbf{W} \\ \mathcal{H}_1 &: \boldsymbol{\Upsilon} = \sqrt{P_p}\ \mathbf{H}_p\boldsymbol{x} + \ \mathbf{W} \\ \mathcal{H}_2 &: \boldsymbol{\Upsilon} = \sqrt{\eta P_{\mathrm{s}}}\ \mathbf{H}_s\boldsymbol{x} + \ \mathbf{W} \\ \mathcal{H}_3 &: \boldsymbol{\Upsilon} = \sqrt{P_p}\ \mathbf{H}_p\boldsymbol{x} + \sqrt{\eta P_s}\ \mathbf{H}_s\boldsymbol{s} + \ \mathbf{W} \end{aligned} \tag{33}$$

where $\mathbf{H}_p$ represents the channel matrix between the transmitter of primary IoT user and the sensing antennas of secondary IoT user (i.e., sensing channel matrix), $\mathbf{H}_s$ represents the channel matrix between the transmitter of secondary IoT user and the sensing antennas of secondary IoT user (i.e., self-interference channel matrix), $\mathbf{x}$ denotes the transmission

signals of the primary IoT user communication link, $\boldsymbol{s}$ represents the residual self-interference signals, and $\mathbf{W}$ is the matrix of the generalized stationary complex-colored Gaussian noise at the receiving end of the secondary IoT user.

Given M orders vectors $\{k_1, \ldots, k_M\}$ and corresponding M lag vectors $\{\boldsymbol{\tau}_1, \ldots, \boldsymbol{\tau}_M\}$, and according to (4) and (9), the estimated multiple high-order cumulants matrix of all the received signals from K sensing antennas can be expressed as

$$\hat{\boldsymbol{\mathcal{U}}}_{k\Upsilon}(\boldsymbol{\tau}) \triangleq \left[\hat{\boldsymbol{u}}_{k\Upsilon_1}(\boldsymbol{\tau}), \ldots, \hat{\boldsymbol{u}}_{k\Upsilon_K}(\boldsymbol{\tau})\right]^T. \tag{34}$$

Then according to (34), by calculating the estimated multiple kth order cumulants for the received sample data during a spectrum sensing period and ignoring the delay parameter vector $\boldsymbol{\tau}$ for simplicity, (33) can be reconstructed as

$$\begin{aligned}
\mathcal{H}_0 &: \hat{\boldsymbol{\mathcal{U}}}_{k\Upsilon} = \boldsymbol{\Delta}_{k\Upsilon}^{(N)} \\
\mathcal{H}_1 &: \hat{\boldsymbol{\mathcal{U}}}_{k\Upsilon} = P_p^{k/2}\boldsymbol{\mathcal{U}}_{kp} + \boldsymbol{\Delta}_{k\Upsilon}^{(N)} \\
\mathcal{H}_2 &: \hat{\boldsymbol{\mathcal{U}}}_{k\Upsilon} = (\eta P_s)^{k/2}\boldsymbol{\mathcal{U}}_{ks} + \boldsymbol{\Delta}_{k\Upsilon}^{(N)} \\
\mathcal{H}_3 &: \hat{\boldsymbol{\mathcal{U}}}_{k\Upsilon} = P_p^{k/2}\boldsymbol{\mathcal{U}}_{kp} + (\eta P_s)^{k/2}\boldsymbol{\mathcal{U}}_{ks} + \boldsymbol{\Delta}_{k\Upsilon}^{(N)}
\end{aligned} \tag{35}$$

where $\boldsymbol{\Delta}_{k\Upsilon}^{(N)}$ is the estimation error matrix. From the foregoing discussion, we know that the asymptotic distribution of $\sqrt{N}\boldsymbol{\Delta}_{k\Upsilon}^{(N)}$ is $\mathcal{N}(\mathbf{0}, \boldsymbol{\Sigma})$.

Similarly, the four hypotheses are divided into two cases according to whether the secondary IoT user transmits signals. In case I, we have

$$\begin{aligned}
\mathcal{H}_0 &: \hat{\boldsymbol{\mathcal{U}}}_{k\Upsilon} = \boldsymbol{\Delta}_{k\Upsilon}^{(N)} \\
\mathcal{H}_1 &: \hat{\boldsymbol{\mathcal{U}}}_{k\Upsilon} = P_p^{k/2}\boldsymbol{\mathcal{U}}_{kp} + \boldsymbol{\Delta}_{k\Upsilon}^{(N)}.
\end{aligned} \tag{36}$$

While, in case II, we have

$$\begin{aligned}
\mathcal{H}_2 &: \hat{\boldsymbol{\mathcal{U}}}_{k\Upsilon} = (\eta P_s)^{k/2}\boldsymbol{\mathcal{U}}_{ks} + \boldsymbol{\Delta}_{k\Upsilon}^{(N)} \\
\mathcal{H}_3 &: \hat{\boldsymbol{\mathcal{U}}}_{k\Upsilon} = P_p^{k/2}\boldsymbol{\mathcal{U}}_{kp} + (\eta P_s)^{k/2}\boldsymbol{\mathcal{U}}_{ks} + \boldsymbol{\Delta}_{k\Upsilon}^{(N)}.
\end{aligned} \tag{37}$$

Apparently, in either case, whether or not the primary IoT user is working will change the mean of $\hat{\boldsymbol{\mathcal{U}}}_{k\Upsilon}$, but not the variance, which conforms to the conditions of Hotelling's T^2-statistic to distinguish the two hypotheses in each case. An introduction to Hotelling's T^2-statistic is described in the following section.

B. Statistical Law of Hotelling's T^2-Statistic

Definition 2: Consider a test of the hypothesis $\mathcal{H}_0 : \boldsymbol{\mu} = \boldsymbol{\mu}_0$ versus $\mathcal{H}_1 : \boldsymbol{\mu} \neq \boldsymbol{\mu}_0$, i.e., determining whether a specific value $\boldsymbol{\mu}_0$ is a plausible value for the population mean $\boldsymbol{\mu}$. By constructing Hotelling's T^2-statistic expressed as $T^2 = K(\bar{\boldsymbol{x}} - \boldsymbol{\mu}_0)\boldsymbol{S}^{-1}(\bar{\boldsymbol{x}} - \boldsymbol{\mu}_0)^H$, where $\bar{\boldsymbol{x}}$ is sample mean, at the α level of significance, we reject $\mathcal{H}_0$ in favor of $\mathcal{H}_1$ if the following inequality satisfied [45, Ch. 5]

$$\begin{aligned}
T^2 &= K\big(\bar{\boldsymbol{x}} - \boldsymbol{\mu}_0\big)\boldsymbol{S}^{-1}\big(\bar{\boldsymbol{x}} - \boldsymbol{\mu}_0\big)^H \\
&> (K-1)M/.(K-M)F_{M,K-M}^{(\alpha)}
\end{aligned} \tag{38}$$

where $F_{M,K-M}^{(\alpha)}$ is the $\mathcal{F}$ value for central F distribution with M, $(K-M)$ degrees of freedom when the probability is equal to α.

According to the definition 2, statistical Law of Hotelling's T^2-statistic can be got from the lemma below.

Lemma 1: If samples $[\boldsymbol{y}_1, \ldots, \boldsymbol{y}_{\mathrm{m}}] \sim \mathcal{N}(\boldsymbol{\mu}, \boldsymbol{\Sigma})$, where $\boldsymbol{y}_i = [y_1, \ldots, y_p]^H$, and construct $T^2 = m(\bar{\boldsymbol{y}} - \boldsymbol{\mu}_0)\boldsymbol{S}^{-1}(\bar{\boldsymbol{y}} - \boldsymbol{\mu}_0)^H$. Then, the distribution of $[T^2/(m-1)][(m-p)/p]$ is noncentral F-distribution with p and $m-p$ degrees of freedom and noncentrality parameter $m(\boldsymbol{\mu} - \boldsymbol{\mu}_0)\boldsymbol{S}^{-1}(\boldsymbol{\mu} - \boldsymbol{\mu}_0)^H$. If $\boldsymbol{\mu} = \boldsymbol{\mu}_0$, then the F-distribution is central.

C. Detection of Primary IoT User's Working State

When multiple sensing antennas are available at the secondary IoT user, we use Hotelling's T^2-statistic to judge whether the primary IoT user is active or not in each case.

In case I, Hotelling's T^2-statistic can be constructed into (39), which is used as test statistics in case I

$$\mathcal{M}_{\mathrm{I}} \triangleq K\bar{\hat{\boldsymbol{u}}}_{k\Upsilon}\boldsymbol{S}_{\mathrm{I}}^{-1}\bar{\hat{\boldsymbol{u}}}_{k\Upsilon}^H \tag{39}$$

where $\bar{\hat{\boldsymbol{u}}}_{k\Upsilon} \triangleq (\sum_{i=1}^{K}\hat{\boldsymbol{u}}_{k\Upsilon_i})/K$ and $\boldsymbol{S}_{\mathrm{I}} \triangleq (\sum_{i=1}^{K}(\hat{\boldsymbol{u}}_{k\Upsilon_i} - \bar{\hat{\boldsymbol{u}}}_{k\Upsilon})^H(\hat{\boldsymbol{u}}_{k\Upsilon_i} - \bar{\hat{\boldsymbol{u}}}_{k\Upsilon}))/(K-1)$. According to the above lemma (Lemma 1), the distribution of the test statistic $\mathcal{M}_{\mathrm{I}}$ can be obtained as

$$\frac{K-M}{(K-1)M}\mathcal{M}_{\mathrm{I}} \sim \begin{cases} F_{M,K-M}, & \mathcal{H}_0 \\ F_{M,K-M}(\lambda_{\mathrm{I}}), & \mathcal{H}_1 \end{cases}. \tag{40}$$

where $\lambda_{\mathrm{I}} = K(P_p^{k/2}\boldsymbol{u}_{kp})\boldsymbol{\Sigma}^{-1}(P_p^{k/2}\boldsymbol{u}_{kp})^H$, whose estimate with finite samples is $\hat{\lambda}_{\mathrm{I}} = \mathcal{M}_{\mathrm{I}} = K\bar{\hat{\boldsymbol{u}}}_{k\Upsilon}\boldsymbol{S}_{\mathrm{I}}^{-1}\bar{\hat{\boldsymbol{u}}}_{k\Upsilon}^H$

To control false-alarm probability as small as possible, the NP criterion is used. If we set Pr_{fa} to be less than δ_{I}, and from (40), the corresponding detection threshold can be calculated as

$$\mathcal{G}_{\mathrm{MMCS}}^{\mathrm{I}} = \frac{(K-1)M}{K-M}F_{M,K-M}^{(\delta_{\mathrm{I}})} \tag{41}$$

where $F_{M,K-M}^{(\delta_{\mathrm{I}})}$ is the $\mathcal{F}$ value for central F distribution with M, K_M degrees of freedom when the probability is equal to δ_{I}.

When the primary IoT user is in the state of communication, the distribution of the test statistic $\mathcal{M}_{\mathrm{I}}$ under $\mathcal{H}_1$ is noncentral F-distribution presented in (40). Noting that the exact PDF of noncentral F distribution is defined as weighted sum of infinite terms, which makes it difficult to directly apply in practice. Considering the theory of uniformly asymptotic normality of noncentral F-distribution, we properly choose the Gaussian distribution to approximate the noncentral F distribution. Specifically, the distribution of noncentral F-distribution $\mathrm{Pr}(F'|v_1, v_2, \lambda)$ can be approximated by [46, Ch. 26, eq. (26.6.27)]

$$\begin{aligned}
&\mathrm{Pr}\big(F'|v_1, v_2, \lambda\big) \approx \mathrm{Pr}(x) \\
&x = \frac{\left[\frac{v_1F'}{(v_1+\lambda)}\right]^{1/3}\left[1 - \frac{2}{9v_2}\right] - \left[1 - \frac{2(v_1+2\lambda)}{9(v_1+\lambda)^2}\right]}{\left[\frac{2(v_1+2\lambda)}{9(v_1+\lambda)^2} + \frac{2}{9v_2}\left(\frac{v_1F'}{(v_1+\lambda)}\right)^{2/3}\right]^{1/2}}
\end{aligned} \tag{42}$$

where $\Pr(x)$ is normal distribution. Then, substituting (41) into (42), the detection probability can be calculated as

$$\Pr_{\mathrm{d1}} = Q\left(\frac{\left[\frac{MF^{(\delta_{\mathrm{I}})}_{M,K-M}}{(M+\mathcal{M}_{\mathrm{I}})}\right]^{1/3}\left[1-\frac{2}{9(K-M)}\right]-\left[1-\frac{2(M+2\mathcal{M}_{\mathrm{I}})}{9(M+\mathcal{M}_{\mathrm{I}})^2}\right]}{\left[\frac{2(M+2\mathcal{M}_{\mathrm{I}})}{9(M+\mathcal{M}_{\mathrm{I}})^2}+\frac{2}{9(K-M)}\left(\frac{MF^{(\delta_{\mathrm{I}})}_{M,K-M}}{(M+\mathcal{M}_{\mathrm{I}})}\right)^{2/3}\right]^{1/2}}\right). \tag{43}$$

In case II, the test statistics can be constructed as

$$\mathcal{M}_{\mathrm{II}} \triangleq K\left(\bar{\hat{\boldsymbol{u}}}_{k\Upsilon}-\bar{\boldsymbol{u}}_{ks}\right)\boldsymbol{S}_{\mathrm{II}}^{-1}\left(\bar{\hat{\boldsymbol{u}}}_{k\Upsilon}-\bar{\boldsymbol{u}}_{ks}\right)^{H} \tag{44}$$

where $\bar{\boldsymbol{u}}_{ks} \triangleq (\eta P_s)^{k/2}(\sum_{i=1}^{K}\boldsymbol{u}_{ks_i})/K$ and $S_{\mathrm{II}} \triangleq (\sum_{i=1}^{K}(\hat{\boldsymbol{u}}_{k\Upsilon_i}-\bar{\hat{\boldsymbol{u}}}_{k\Upsilon})^{H}(\hat{\boldsymbol{u}}_{k\Upsilon_i}-\bar{\hat{\boldsymbol{u}}}_{k\Upsilon}))/(K-1)$. According to the Lemma 1, the distribution of the test statistic $\mathcal{M}_{\mathrm{II}}$ can be obtained as

$$\frac{K-M}{(K-1)M}\mathcal{M}_{\mathrm{II}} \sim \begin{cases} F_{M,K-M}, & \mathcal{H}_2 \\ F_{M,K-M}(\lambda_{II}), & \mathcal{H}_3 \end{cases} \tag{45}$$

where $\lambda_{II} = K(P_p^{k/2}\boldsymbol{u}_{kp})\boldsymbol{\Sigma}^{-1}(P_p^{k/2}\boldsymbol{u}_{kp})^H$, whose estimate in a finite sample is $\hat{\lambda}_{II} = \mathcal{M}_{\mathrm{II}} = K(\bar{\hat{\boldsymbol{u}}}_{k\Upsilon}-\bar{\hat{\boldsymbol{u}}}_{ks})\boldsymbol{S}_{\mathrm{II}}^{-1}(\bar{\hat{\boldsymbol{u}}}_{k\Upsilon}-\bar{\hat{\boldsymbol{u}}}_{ks})^H$. Similarly, leveraging the NP criterion, we set $\Pr_{fa}$ to be less than δ_{II}, and from (45), the corresponding detection threshold can be calculated as

$$\mathcal{G}^{\mathrm{II}}_{\mathrm{MMCS}} = \frac{(K-1)M}{K-M}F^{(\delta_{II})}_{M,K-M} \tag{46}$$

where $F^{(\delta_{II})}_{M,K-M}$ is the $\mathcal{F}$ value for central F distribution with M, $K-M$ degrees of freedom when the probability is equal to δ_{II}. As defined in (41) and (46), the thresholds in both cases are related to preset values M, $K-M$, δ_I, and δ_{II}, with the result that the proposed MMCS scheme is nonparametric and also unaffected by noise uncertainty.

Then, applying (46) into (42), the estimated value of detection probability in case II is

$$\Pr_{\mathrm{d2}} = Q\left(\frac{\left[\frac{MF^{(\delta_{II})}_{M,K-M}}{(M+\mathcal{M}_{\mathrm{II}})}\right]^{1/3}\left[1-\frac{2}{9(K-M)}\right]-\left[1-\frac{2(M+2\mathcal{M}_{\mathrm{II}})}{9(M+\mathcal{M}_{\mathrm{II}})^2}\right]}{\left[\frac{2(M+2\mathcal{M}_{\mathrm{II}})}{9(M+\mathcal{M}_{\mathrm{II}})^2}+\frac{2}{9(K-M)}\left(\frac{MF^{(\delta_{II})}_{M,K-M}}{(M+\mathcal{M}_{\mathrm{II}})}\right)^{2/3}\right]^{1/2}}\right). \tag{47}$$

In summary, the proposed MMCS scheme has five steps as follows.

Step 1: Based on N samples of each sensing antenna, the received signals from the secondary IoT user outfitted with K sensing antennas can be constructed to form a receiving signal matrix. According to the working status of the secondary IoT user, determine whether this test process is in case I or case II.

Step 2: Compute the estimated multiple high-order cumulant matrix $\hat{\boldsymbol{\mathcal{U}}}_{k\Upsilon}$.

Step 3: Compute the estimated mean $\bar{\hat{\boldsymbol{u}}}_{k\Upsilon}$ and estimated covariance matrix $\boldsymbol{S}_{\mathrm{I}}$ in case I or $\boldsymbol{S}_{\mathrm{II}}$ in case II, separately.

Step 4: Construct test statistics $\mathcal{M}_{\mathrm{I}}$ or $\mathcal{M}_{\mathrm{II}}$ according to (39) or (44), respectively.

Step 5: Preset false-alarm probability $\Pr_{fa}$. Then, set up the detection threshold $\mathcal{G}^{\mathrm{I}}_{\mathrm{MMCS}}$ or $\mathcal{G}^{\mathrm{II}}_{\mathrm{MMCS}}$ according to (41) or (46) with $\Pr_{fa}$ preset. By comparing test statistics with detection threshold, we can determine the working state of primary IoT user.

D. Computational Complexity of MMCS Scheme

When it comes to the computational complexity of the MMCS scheme, the computational complexity required for getting the estimated k-order cumulants from K antennas are $K\sum_{i=1}^{M}v_i(k_i-1)N$ multiplications and $K\sum_{i=1}^{M}\sum_{r=1}^{v_i}m_r(N-1)$ additions. While only $K+1$ multiplications and $3K-1$ additions are needed for the estimated covariance matrix $\boldsymbol{S}_{\mathrm{I}}$ or $\boldsymbol{S}_{\mathrm{II}}$.

Compared to the sample size N, the number of antennas K is often quite small, which means that the computational complexity of the MMCS scheme is much less than the computational complexity of the MCS scheme. However, the computational complexity is reduced at the expense of detection accuracy. Because in the MMCS scheme, the characteristics of the non-Gaussian signals are extracted by high-order cumulants only, then the test statistics are constructed by statistical hypothesis testing, and the estimated sample variance is used in the specific calculation. Furthermore, the diversity of multiple antennas in space is not utilized. Nevertheless, the MMCS scheme allows for a tradeoff between performance and computational complexity.

VI. Simulation Results

In this section, simulation results are presented to evaluate the performance of the proposed two sensing schemes in FD-enabled CR-IoT networks. The transmission signals of both the primary IoT users and secondary IoT users considered in the simulation are QPSK signals. The symbol rate is 1 MHz and the sampling frequency is set as 6 times the symbol rate, i.e., 6 MHz. We assume that the spectrum access procedure of primary IoT user is modeled as an NTS alternating ON/OFF process with full transmission power of primary IoT user denoted as P_p. Furthermore, P_s and η reflects the transmission signal power and SIS ability of the secondary IoT user, respectively. More specifically, $\eta \in [0, 1]$, where $\eta = 0$ indicates that the secondary IoT user can completely suppress the detrimental effect of the transmission signal from itself, and $\eta = 1$ indicates that there is no self-interference suppression taken by the secondary IoT user at all. Then, the residual self-interference at each sensing antenna of the secondary IoT user is denoted by $\sqrt{\eta P_s}h_s(n)s(n)$. As discussed in [26, Ch. 9], the colored Gaussian noise $w(n)$ is assumed to be correlated with $a = -0.9$ and $\sigma_w^2 = 1$, that is $w(n) = 0.9w(n-1)+u(n)$, where $u(n)$ is the white Gaussian noise (WGN) with zero mean and unit variance. Then, the SNR is defined as P/σ_w^2. When noise uncertainty exists, noise variance is no longer a

constant, but a random variable that follows a uniform distribution in $[\sigma_w^2/\xi, \sigma_w^2\xi]$, where ξ is the noise uncertainty factor. Let $\rho = 10\log_{10}\xi$ represent the noise uncertainty factor in dB. In the legend of the simulation diagram, Pr_d and Pr_{fa} are used to indicate the detection probability and false-alarm probability, respectively. According to the latest method proposed in [47], the SIS performance can reach approximately 54 dB cancelation. Then, we set $\eta = 0.01$ and the SNR of secondary IoT user $\mathrm{SNR_s} = 0$ dB in the simulation unless otherwise specified. All the simulation results are obtained and averaged from 10 000 Monte Carlo runs.

According to [48], the fourth-order cumulants of digital modulated signals tend to 0 as the time lag τ increases. Therefore, in the following simulations, we use fourth-order cumulants with $\boldsymbol{\tau}_1 = [0, 0, 0]$ and $\boldsymbol{\tau}_2 = [0, 0, 1]$ to processing transmission signals, which can extract the non-Gaussian transmission signals from the Gaussian noise felicitously. Specially, the variances of estimated fourth-order cumulants $\hat{u}_4(\boldsymbol{\tau}_1)$ and $\hat{u}_4(\boldsymbol{\tau}_2)$ and the covariance between them can be estimated as

$$\begin{aligned} &N\mathrm{var}\big[\hat{u}_4(\boldsymbol{\tau}_1)\big] \\ &\quad = \hat{\mathcal{D}}_{4,4}(\boldsymbol{\tau}_1, \boldsymbol{\tau}_1) - 12\hat{\mathcal{D}}_{4,2}(\boldsymbol{\tau}_1, 0)\hat{\zeta}_{2x}(0) \\ &\qquad + 36\hat{\mathcal{D}}_{2,2}(0, 0)\hat{\zeta}_{2x}(0)\hat{\zeta}_{2x}(0) \end{aligned} \tag{48}$$

$$\begin{aligned} &N\mathrm{var}\big[\hat{u}_4(\boldsymbol{\tau}_2)\big] \\ &\quad = \hat{\mathcal{D}}_{4,4}(\boldsymbol{\tau}_2, \boldsymbol{\tau}_2) - 6\hat{\mathcal{D}}_{4,2}(\boldsymbol{\tau}_2, 0)\hat{\zeta}_{2x}(1) \\ &\qquad - 6\hat{\mathcal{D}}_{4,2}(\boldsymbol{\tau}_2, 1)\hat{\zeta}_{2x}(0) + 9\hat{\mathcal{D}}_{2,2}(0, 0)\hat{\zeta}_{2x}(1)\hat{\zeta}_{2x}(1) \\ &\qquad + 18\hat{\mathcal{D}}_{2,2}(0, 1)\hat{\zeta}_{2x}(0)\hat{\zeta}_{2x}(1) + 9\hat{\mathcal{D}}_{2,2}(1, 1)\hat{\zeta}_{2x}(0)\hat{\zeta}_{2x}(0) \end{aligned} \tag{49}$$

$$\begin{aligned} &N\mathrm{var}\big[\hat{u}_4(\boldsymbol{\tau}_1), \hat{u}_4(\boldsymbol{\tau}_2)\big] \\ &\quad = \hat{\mathcal{D}}_{4,4}(\boldsymbol{\tau}_1, \boldsymbol{\tau}_2) - 6\hat{\mathcal{D}}_{4,2}(\boldsymbol{\tau}_2, 0)\hat{\zeta}_{2x}(0) \\ &\qquad - 3\hat{\mathcal{D}}_{4,2}(\boldsymbol{\tau}_1, 0)\hat{\zeta}_{2x}(1) - 3\hat{\mathcal{D}}_{4,2}(\boldsymbol{\tau}_1, 1)\hat{\zeta}_{2x}(0) \\ &\qquad + 18\hat{\mathcal{D}}_{2,2}(0, 0)\hat{\zeta}_{2x}(0)\hat{\zeta}_{2x}(1) + 18\hat{\mathcal{D}}_{2,2}(0, 1)\hat{\zeta}_{2x}(0)\hat{\zeta}_{2x}(0). \end{aligned} \tag{50}$$

Fig. 2 shows the theoretical value and simulation value for detection probability Pr_d of the MCS scheme versus sample number with SNR $= -6, -8$dB. We set the false-alarm probability $\mathrm{Pr}_{fa} = 0.01$. It can be seen that the detection probability increases with sample number. Besides, the theoretical value curve and simulation value curve tend to coincide when the sample number is large enough, which is mainly due to the asymptotic Gaussian distribution used in the derivation of (13) and (15). When the number of received samples is large, asymptotic results are closer to accurate results. In spite of approximation, the gap between the theoretical value and the simulation value is acceptable.

Fig. 3 depicts the theoretical value and simulation value for detection probability Pr_d of the MMCS scheme versus sample number with SNR $= -3, -5$ dB, $M = 2$ and the number of spectrum sensing antennas $K = 5$. We also set the false-alarm probability $\mathrm{Pr}_{fa} = 0.01$. It can be seen that the detection probability rises with sample number, and the theoretical value curve approaches the simulation value curve as the number of samples increases. Moreover, when the number of samples is small, the gap between the simulation value and the theoretical

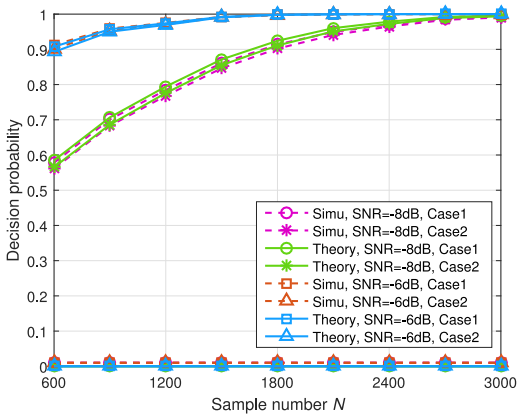

Fig. 2. Pr_d of the MCS scheme versus sample number with SNR $= -6, -8$ dB.

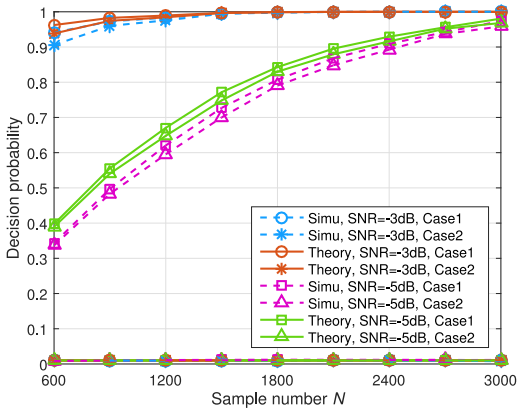

Fig. 3. Pr_d of the MMCS scheme versus sample number with SNR $= -3, -5$ dB, $M = 2$, and $K = 5$.

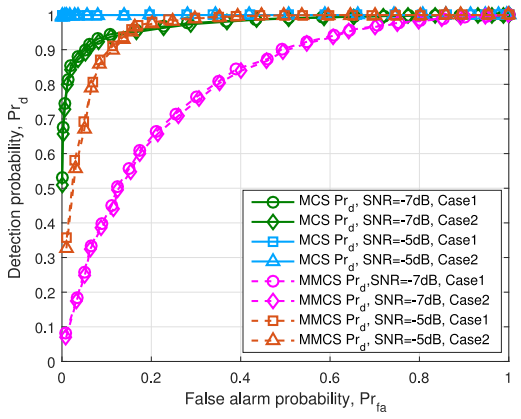

Fig. 4. ROC curves of the MCS scheme and MMCS scheme with sample number equaling to 800, $M = 2$, and $K = 5$.

value is large. This is mainly due to two reasons. On one hand, the MMCS scheme uses the asymptotic Gaussian distribution to derive test statistics. On the other hand, the statistical sample variance instead of theoretical variance is used in the MMCS scheme. When the number of samples is small, the difference between the sample variance and the theoretical value is large.

Fig. 4 illustrates the ROC curves of MCS scheme and MMCS scheme with the sample number equalling 800, $M = 2$, and $K = 5$. The false-alarm probability curves ascend relatively stable on the grounds of enough samples, which verifies

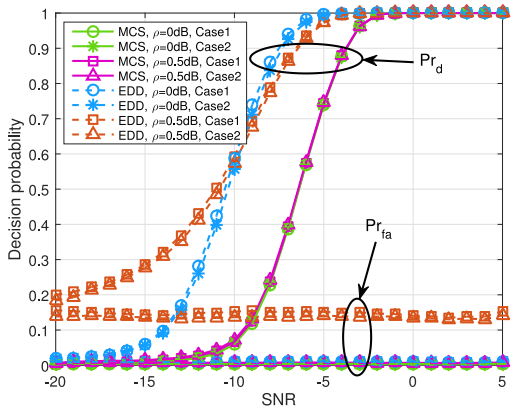

Fig. 5. Impact of noise uncertainty on the MCS method and EDD method versus SNR with sample number equaling to 800 and $\mathrm{Pr}_{fa} = 0.01$.

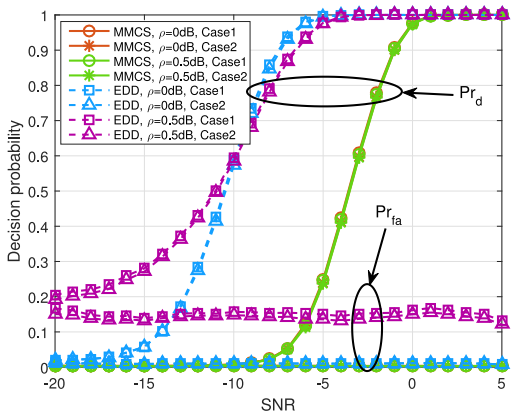

Fig. 6. Impact of noise uncertainty on MMCS method and EDD method versus SNR with sample number equaling to 800, $\mathrm{Pr}_{fa} = 0.01$, $M = 2$, and $K = 5$.

the rationality of the proposed two methods. In addition, it can be clearly seen from Fig. 4 that the MCS has superiority over MMCS in terms of sensing performance. This is because, in the absence of prior information, the MCS scheme obtains the near-optimal solution via LRT. In contrast, although high-order cumulants are also used in the MMCS scheme to extract the non-Gaussian characteristics of signals, statistical hypothesis tests are used in constructing test statistics, and the sample variance is used to approximate the true variance. In addition, the MMCS scheme does not use the spatial complexity of multiple antennas. These factors make MCS scheme much better than MMCS scheme in terms of detection probability.

Fig. 5 presents the impact of noise uncertainty on the MCS method and EDD method [30] versus SNR with sample number equaling 800. We set $\mathrm{Pr}_{fa} = 0.01$ and noise uncertainty factor $\rho = 0.5$dB. From Fig. 5, the contrast between the two methods is extremely obvious when the noise uncertainty exists. Apparently, the detection probability curves and false-alarm probability curves of the MCS method are almost identical whether there is noise uncertainty or not, which indicates that the proposed MCS scheme is robust to noise uncertainty. This is due to the fact that the high-order cumulants higher than the second order are all 0 for the Gaussian noise, regardless of whether it is colored or not. Therefore, the decision process of the MCS method is no longer adversely affected by noise uncertainty. In contrast, although the detection probability of EDD is higher than that of the proposed MCS method when there is noise uncertainty, the false-alarm probability curve of energy detection rises obviously. The false-alarm probability of the EDD method rises from 0.01 to 0.15, which means that EDD cannot be used as a reliable detection method when there exists noise uncertainty. Consequently, the proposed MCS method outperforms the EDD method in terms of robustness against noise uncertainty.

Fig. 6 shows the impact of noise uncertainty on the MMCS method and EDD method [30] versus SNR with sample number equaling 800. We set $\mathrm{Pr}_{fa} = 0.01$, $M = 2$, $K = 5$, and noise uncertainty factor $\rho = 0.5$ dB. Observing the detection performance of the MMCS method with and without noise uncertainty, the detection probability curves almost overlap

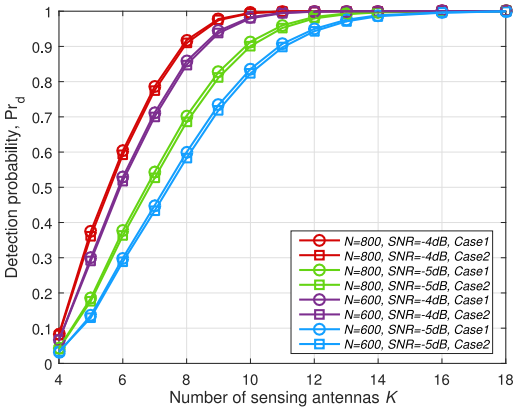

Fig. 7. Detection probability of the MMCS method versus K with SNR $= -4, -5$ dB, $M = 2$, and $\mathrm{Pr}_{fa} = 0.01$.

and the false-alarm probability curves are steadily kept at a very low level. This is due to two aspects. On one hand, cumulants higher than the second-order are all 0 for the Gaussian noise. On the other hand, the detection threshold of the binary hypothesis test constructed by Hotelling's T^2-statistic is nonparametric and not affected by the noise power. Additionally, it is obvious that the MMCS method can also resist the negative impact of noise uncertainty and has better performance than EDD in terms of robustness to noise uncertainty.

Fig. 7 illustrates the detection probability curves of MMCS method versus K. We set SNR $= -4, -5$ dB, $M = 2$, and $\mathrm{Pr}_{fa} = 0.01$. Since the MMCS method requires $K > M$, the curves do not start at the origin. The detection probability ascends with the increase of K until the optimal detection is achieved. This is because in hypothesis testing, more antennas can promote the multiple high-order cumulants to extract richer statistical information of signals. So, the more antennas there are, the better the detection performance will be until the detection performance reaches the optimal level.

Fig. 8 presents the impact of residual self-interference on MCS method and MMCS method with sample number equaling 800, $M = 2$, and $K = 5$. It can be seen from Fig. 8 that the detection probability of the MCS method is higher than that of the MMCS method under the same degree of SIS, i.e.,

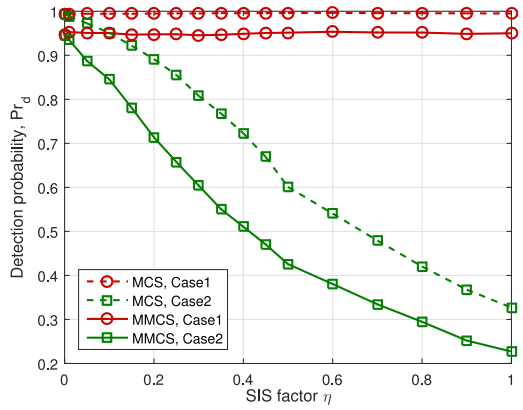

Fig. 8. Impact of residual self-interference on MCS method and MMCS method with sample number equaling to 800, $M = 2$, and $K = 5$.

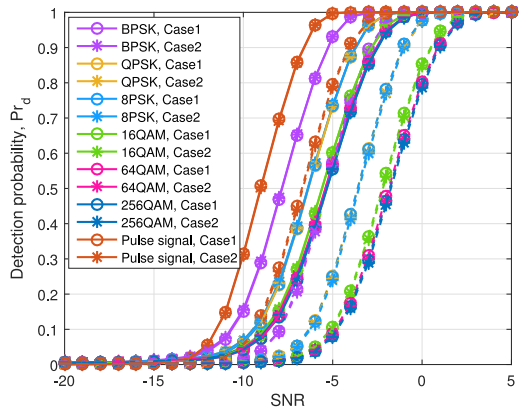

Fig. 9. Detection probability of the proposed schemes for various typical non-Gaussian signals.

η value. However, the residual self-interference will deteriorate the detection performance of the two methods, and the decline trend of the two methods is basically the same. This is because poor SIS will lead to higher residual self-interference, which will decrease the signa-to-interference-plus-noise ratio and then deteriorate the detection performance.

Fig. 9 shows the detection probability of the MCS and MMCS schemes for various typical non-Gaussian signals with sample number equaling to 800, in which the solid line represents the detection probability of the MCS scheme, and the dotted line demonstrates the detection probability of MMCS scheme. The pulse width of pulse signals is set as 1 μs, and the pulse repetition interval is set as 10 μs. The symbol rate of the all the modulated signal is 1 MHz. It can be seen from Fig. 9 that both the proposed schemes are valid for the adopted non-Gaussian signals. In detail, when the pulse signal is used by the primary transmitter, both the proposed two detection schemes perform well. As for the digital modulated signals, the detection probabilities of both MCS and MMCS schemes decrease with the increase of the modulation order of signals. This is due to the fact that a higher modulation order means a larger constellations, which leads the transmitted modulated signal tends to Gaussian process. Nevertheless, both the proposed MCS and MMCS schemes can detect the non-Gaussian primary transmitted signals by excavating the high order cumulants.

VII. Conclusion

In this article, we have proposed two multiple high-order cumulants-based spectrum sensing method for FD-enabled CR-IoT networks, considering the secondary IoT users equipped with multiple sensing antennas and the non-Gaussian transmitted signals used by the primary as well as secondary IoT users. Additionally, two cases are considered for studying each method corresponding to the state whether the cognitive IoT user is silent or active. Specifically, when only a single antenna is available at the secondary IoT user, the MCS method has been designed with LRT to pursue near optimum in theory and low hardware overhead. Furthermore, the closed-form expression of the decision threshold was obtained by using NP criterion. Then, when multiple sensing antennas are available at the secondary IoT user, the MMCS method has been proposed with Hotelling's T^2-statistic used as test statics. The MMCS method has lower computational complexity than the MCS method, while the sensing performance was also degraded compared to the MCS method. Nevertheless, MMCS method provides a compromise between computational complexity and sensing performance. In addition, the two methods can resist the negative effects of noise uncertainty, but when the SIS is poor, the sensing performance of the proposed two methods will be degraded due to strong self-interference. Finally, numerical results have been provided to verify the theoretical analysis and evaluate the performance of the proposed scheme.

For future work, we will investigate the interference signal identification in FD cognitive IoT system, considering multiple time-varying frequencies of potential interference signals.

References

[1] L. Chettri and R. Bera, "A comprehensive survey on Internet of things(IoT) toward 5G wireless systems," *IEEE Internet Things J.*, vol. 7, no. 1, pp. 16–32, Jan. 2020.

[2] J. G. Andrews *et al.*, "What will 5G be?" *IEEE J. Sel. Areas Commun.*, vol. 32, no. 6, pp. 1065–1082, Jun. 2014.

[3] Q. Liang, T. S. Durrani, X. Gu, J. Koh, Y. Li, and X. Wang, "Guest editorial special issue on spectrum and energy efficient communications for Internet of things," *IEEE Internet Things J.*, vol. 6, no. 4, pp. 5948–5953, Aug. 2019.

[4] N. Zhang, N. Cheng, N. Lu, H. Zhou, J. W. Mark, and X. S. Shen, "Risk-aware cooperative spectrum access for multi-channel cognitive radio networks," *IEEE J. Sel. Areas Commun.*, vol. 32, no. 3, pp. 516–527, Mar. 2014.

[5] J. Adu Ansere, G. Han, H. Wang, C. Choi, and C. Wu, "A reliable energy efficient dynamic spectrum sensing for cognitive radio IoT networks," *IEEE Internet Things J.*, vol. 6, no. 4, pp. 6748–6759, Aug. 2019.

[6] L. Chettri and R. Bera, "A comprehensive survey on Internet of things (IoT) toward 5G wireless systems," *IEEE Internet Things J.*, vol. 7, no. 1, pp. 16–32, Jan. 2020.

[7] N. Zhang, H. Liang, N. Cheng, Y. Tang, J. W. Mark, and X. S. Shen, "Dynamic spectrum access in multi-channel cognitive radio networks," *IEEE J. Sel. Areas Commun.*, vol. 32, no. 11, pp. 2053–2064, Nov. 2014.

[8] C. Perera, A. Zaslavsky, P. Christen, and D. Georgakopoulos, "Context aware computing for the Internet of things: A survey," *IEEE Commun. Surveys Tuts.*, vol. 16, no. 1, pp. 414–454, 1st Quart., 2014.

[9] N. Zhang, N. Lu, N. Cheng, J. W. Mark, and X. S. Shen, "Cooperative spectrum access towards secure information transfer for CRNs," *IEEE J. Sel. Areas Commun.*, vol. 31, no. 11, pp. 2453–2464, Nov. 2013.

[10] C. Liu, J. Wang, X. Liu, and Y.-C. Liang, "Deep CM-CNN for spectrum sensing in cognitive radio," *IEEE J. Sel. Areas Commun.*, vol. 37, no. 10, pp. 2306–2321, Oct. 2019.

[11] E. Lagunas, S. K. Sharma, S. Maleki, S. Chatzinotas, and B. Ottersten, "Resource allocation for cognitive satellite communications with incumbent terrestrial networks," *IEEE Trans. Cogn. Commun. Netw.*, vol. 1, no. 3, pp. 305–317, Sep. 2015.

[12] W. Cheng, X. Zhang, and H. Zhang, "Full-duplex spectrum-sensing and MAC-protocol for multichannel nontime-slotted cognitive radio networks," *IEEE J. Sel. Areas Commun.*, vol. 33, no. 5, pp. 820–831, May 2015.

[13] M. Amjad, F. Akhtar, M. H. Rehmani, M. Reisslein, and T. Umer, "Full-duplex communication in cognitive radio networks: A survey," *IEEE Commun. Surveys Tuts.*, vol. 19, no. 4, pp. 2158–2191, 4th Quart., 2017.

[14] D. Kim, H. Lee, and D. Hong, "A survey of in-band full-duplex transmission: From the perspective of PHY and MAC layers," *IEEE Commun. Surveys Tuts.*, vol. 17, no. 4, pp. 2017–2046, 4th Quart., 2015.

[15] T. Riihonen, S. Werner, and R. Wichman, "Mitigation of loopback self-interference in full-duplex MIMO relays," *IEEE Trans. Signal Process.*, vol. 59, no. 12, pp. 5983–5993, Dec. 2011.

[16] E. Tsakalaki, O. N. Alrabadi, A. Tatomirescu, E. de Carvalho, and G. F. Pedersen, "Concurrent communication and sensing in cognitive radio devices: Challenges and an enabling solution," *IEEE Trans. Antennas Propag.*, vol. 62, no. 3, pp. 1125–1137, Mar. 2014.

[17] A. C. Cirik, R. Wang, Y. Rong, and Y. Hua, "MSE-based transceiver designs for full-duplex MIMO cognitive radios," *IEEE Trans. Commun.*, vol. 63, no. 6, pp. 2056–2070, Jun. 2015.

[18] X. Zhang, W. Cheng, and H. Zhang, "Full-duplex transmission in PHY and MAC layers for 5G mobile wireless networks," *IEEE Wireless Commun.*, vol. 22, no. 5, pp. 112–121, Oct. 2015.

[19] Z. Zhang, K. Long, A. V. Vasilakos, and L. Hanzo, "Full-duplex wireless communications: Challenges, solutions, and future research directions," *Proc. IEEE*, vol. 104, no. 7, pp. 1369–1409, Jul. 2016.

[20] S. Hong *et al.*, "Applications of self-interference cancellation in 5G and beyond," *IEEE Commun. Mag.*, vol. 52, no. 2, pp. 114–121, Feb. 2014.

[21] K. E. Kolodziej, B. T. Perry, and J. S. Herd, "In-Band full-duplex technology: Techniques and systems survey," *IEEE Trans. Microw. Theory Techn.*, vol. 67, no. 7, pp. 3025–3041, Jul. 2019.

[22] A. Turlapaty and Y. Jin, "Bayesian sequential parameter estimation by cognitive radar with multiantenna arrays," *IEEE Trans. Signal Process.*, vol. 63, no. 4, pp. 974–987, Feb. 2015.

[23] A. R. Ndjiongue, T. Shongwe, and H. C. Ferreira, "Closed-form BER expressions for HSV-based *M* PSK-CSK systems," *IEEE Commun. Lett.*, vol. 21, no. 5, pp. 1023–1026, May 2017.

[24] X. Liang, Z. Ding, and C. Xiao, "Optimized power allocation for packet retransmissions of non-Gaussian inputs through sequential AWGN channels," *IEEE Trans. Commun.*, vol. 60, no. 7, pp. 1889–1902, Jul. 2012.

[25] R. Tandra and A. Sahai, "SNR walls for signal detection," *IEEE J. Sel. Topics Signal Process.*, vol. 2, no. 1, pp. 4–17, Feb. 2008.

[26] S. M. Kay, *Fundamentals of Statistical Signal Processing, Volume II Detection Theory*, 3rd ed. Englewood Cliffs, NJ, USA: Prentice-Hall, 1998.

[27] Y. Liao, L. Song, Z. Han, and Y. Li, "Full duplex cognitive radio: A new design paradigm for enhancing spectrum usage," *IEEE Commun. Mag.*, vol. 53, no. 5, pp. 138–145, May 2015.

[28] S. Biswas, K. Singh, O. Taghizadeh, and T. Ratnarajah, "Coexistence of MIMO radar and FD MIMO cellular systems with QoS considerations," *IEEE Trans. Wireless Commun.*, vol. 17, no. 11, pp. 7281–7294, Nov. 2018.

[29] C. B. Papadias, T. Ratnarajah, and D. T. M. Slock, *Spectrum Sharing With Full Duplex*. Hoboken, NJ, USA: Wiley, 2019, pp. 191–212.

[30] A. A. Boulogeorgos and G. K. Karagiannidis, "Energy detection in full-duplex systems with residual RF impairments over fading channels," *IEEE Wireless Commun. Lett.*, vol. 7, no. 2, pp. 246–249, Apr. 2018.

[31] P. Karunakaran and W. H. Gerstacker, "Sensing algorithms and protocol for simultaneous sensing and reception-based cognitive D2D communications in LTE-A systems," *IEEE Trans. Cogn. Commun. Netw.*, vol. 4, no. 1, pp. 93–107, Mar. 2018.

[32] M. Deng, B.-J. Hu, and X. Li, "Adaptive weighted sensing with simultaneous transmission for dynamic primary user traffic," *IEEE Trans. Commun.*, vol. 65, no. 3, pp. 992–1004, Mar. 2017.

[33] S. K. Sharma, T. E. Bogale, L. B. Le, S. Chatzinotas, X. Wang, and B. Ottersten, "Dynamic spectrum sharing in 5G wireless networks with full-duplex technology: Recent advances and research challenges," *IEEE Commun. Surveys Tuts.*, vol. 20, no. 1, pp. 674–707, 1st Quart., 2018.

[34] H. Shehata and T. Khattab, "Energy detection spectrum sensing in full-duplex cognitive radio: The practical case of Rician RSI," *IEEE Trans. Commun.*, vol. 67, no. 9, pp. 6544–6555, Sep. 2019.

[35] M. Duarte, C. Dick, and A. Sabharwal, "Experiment-driven characterization of full-duplex wireless systems," *IEEE Trans. Wireless Commun.*, vol. 11, no. 12, pp. 4296–4307, Dec. 2012.

[36] W. Afifi and M. Krunz, "TSRA: An adaptive mechanism for switching between communication modes in full-duplex opportunistic spectrum access systems," *IEEE Trans. Mobile Comput.*, vol. 16, no. 6, pp. 1758–1772, Jun. 2017.

[37] A. Assra, J. Yang, and B. Champagne, "An EM approach for cooperative spectrum sensing in multiantenna CR networks," *IEEE Trans. Veh. Technol.*, vol. 65, no. 3, pp. 1229–1243, Mar. 2016.

[38] R. Zhang, T. J. Lim, Y. Liang, and Y. Zeng, "Multi-antenna based spectrum sensing for cognitive radios: A GLRT approach," *IEEE Trans. Commun.*, vol. 58, no. 1, pp. 84–88, Jan. 2010.

[39] C. Liu, H. Li, J. Wang, and M. Jin, "Optimal eigenvalue weighting detection for multi-antenna cognitive radio networks," *IEEE Trans. Wireless Commun.*, vol. 16, no. 4, pp. 2083–2096, Apr. 2017.

[40] A. McCormick and A. K. Nandi, *Blind Estimation Using Higher-Order Statistics*, 1st ed. Berlin, Germany: Springer, 1999.

[41] D. R. Brillinger, *Time Series: Data Analysis and Theory*, 2nd ed. Philadelphia, PA, USA: SIAM, 1981.

[42] A. V. Dandawate and G. B. Giannakis, "Asymptotic theory of mixed time averages and *k*th-order cyclic-moment and cumulant statistics," *IEEE Trans. Inf. Theory*, vol. 41, no. 1, pp. 216–232, Jan. 1995.

[43] A. V. Dandawate and G. B. Giannakis, "Asymptotic properties and covariance expressions of kth-order sample moments and cumulants," in *Proc. 27th Asilomar Conf. Signals Syst. Comput.*, vol. 2, Nov. 1993, pp. 1186–1190.

[44] R. A. Johnson and D. W. Wichern, *Applied Multivariate Statistical Analysis*, 6th ed. Upper Saddle River, NJ, USA: Pearson Educ., 2007.

[45] T. W. Anderson, *An Introduction to Multivariate Statistical Analysis*, 3rd ed. New York, NY, USA: Wiley, 2003.

[46] M. Abramowitz and I. A. Stegun, *Handbook of Mathematical Functions with Formulas, Graphs, and Mathematical Tables*, 9th ed. Washington, DC, USA: Nat. Bureau Stand., 1970.

[47] K. Komatsu, Y. Miyaji, and H. Uehara, "Iterative nonlinear self-interference cancellation for in-band full-duplex wireless communications under mixer imbalance and amplifier nonlinearity," *IEEE Trans. Wireless Commun.*, vol. 19, no. 7, pp. 4424–4438, Jul. 2020.

[48] D. Wang, N. Zhang, Z. Li, F. Gao, and X. Shen, "Leveraging high order cumulants for spectrum sensing and power recognition in cognitive radio networks," *IEEE Trans. Wireless Commun.*, vol. 17, no. 2, pp. 1298–1310, Feb. 2018.

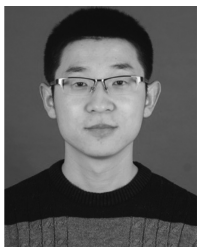

Danyang Wang (Member, IEEE) received the Ph.D. degree in telecommunications engineering from Xidian University, Xi'an, China, in 2017.

He was a Postdoctoral Research Fellow with Xidian University from 2018 to 2020. From 2016 to 2017, he visited the Broadband Communications Research Group, University of Waterloo, Waterloo, ON, Canada. He is currently a Lecturer with Xidian University. His research interests are in the area of cognitive radio networks, cooperative spectrum sensing, covert communication, and machine learning.

Dr. Wang received the Best Paper Awards from IEEE SAGC 2020.

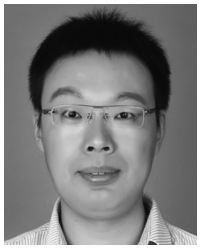

Peihan Qi (Member, IEEE) received the B.S. degree in telecommunications engineering from Chang'an University, Xi'an, China, in 2006, and the M.S. degree in communication and information system and the Ph.D. degree from Xidian University, Xi'an, in 2011 and 2014, respectively.

Since July 2018, he has been an Associate Professor with the School of Telecommunications Engineering, Xidian University. He is interested in compressed sensing, spectrum sensing in cognitive radio networks, and high-speed digital signal processing.

Qifan Fu received the B.S. degree in electronic information science and technology from Jilin University, Changchun, China, in 2017. He is currently pursuing the M.S. degree in information and telecommunications engineering with Xidian University, Xi'an, China.

His research interests are mainly focused on covert communications, signal processing, spectrum sensing, and machine learning for wireless communications.

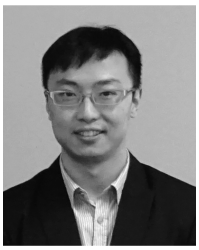

Ning Zhang (Senior Member, IEEE) received the Ph.D. degree in electrical and computer engineering from the University of Waterloo, Waterloo, ON, Canada, in 2015.

He is an Associate Professor with the Department of Electrical and Computer Engineering, University of Windsor, Windsor, ON, Canada. He was a Postdoctoral Research Fellow with the University of Waterloo and University of Toronto, Toronto, ON, Canada. His research interests include connected vehicles, mobile-edge computing, wireless networking, and machine learning.

Dr. Zhang is a Highly Cited Researcher (Web of Science). He received the NSERC PDF Award in 2015 and six Best Paper Awards from IEEE Globecom in 2014, IEEE WCSP in 2015, IEEE ICC in 2019, IEEE ICCC in 2019, IEEE Technical Committee on Transmission Access and Optical Systems in 2019, and *Journal of Communications and Information Networks* in 2018. He serves as an Associate Editor for IEEE INTERNET OF THINGS, IEEE TRANSACTIONS ON COGNITIVE COMMUNICATIONS AND NETWORKING, and IEEE SYSTEMS JOURNAL, and an Guest Editor of several international journals, such as IEEE WIRELESS COMMUNICATIONS, IEEE TRANSACTIONS ON INDUSTRIAL INFORMATICS, IEEE TRANSACTIONS ON INTELLIGENT TRANSPORTATION SYSTEMS, and IEEE TRANSACTIONS ON COGNITIVE COMMUNICATIONS AND NETWORKING. He also serves/served as the TPC Chair for IEEE SAGC 2020, the Track Chair for several international conferences, including IEEE VTC 2020, IEEE ICC 2022, AICON 2020, and CollaborateCom 2020, and the Co-Chair for numerous international workshops.

Zan Li (Senior Member, IEEE) received the B.S. degree in communications engineering and the M.S. and Ph.D. degrees in communication and information systems from Xidian University, Xi'an, China, in 1998, 2001, and 2006, respectively.

She is currently a Professor with the State Key Laboratory of Integrated Services Networks, School of Telecommunications Engineering, Xidian University. Her research interests include topics on wireless communications and signal processing, such as covert communication, spectrum sensing, and cooperative communications.

Prof. Li was awarded the National Science Fund for Distinguished Young Scholars. She serves as an Associate Editor for the IEEE TRANSACTIONS ON COGNITIVE COMMUNICATIONS AND NETWORKING and *China Communications*. She is a Fellow of the Institution of Engineering and Technology, China Institute of Electronics, and China Institute of Communications.